Universidade de Aveiro Departamento de Física
2010

Behabitu Ergette Tebikachew

Preparation of VACNT/PMMA Composites *via* ATRP and Their Characterization

Preparação de Compósitos de VACNT/PMMA *via* ATRP e sua Caracterização

Universidade de Aveiro Departamento de Física
2010

Behabitu Ergette Tebikachew

Preparation of VACNT/PMMA Composites *via* ATRP and Their Characterization

Preparação de Compósitos de VACNT/PMMA *via* ATRP e sua Caracterização

Master thesis submitted to the University of Aveiro for the requirement in the partial fulfilment of Masters of Science degree in Materials Science under the supervision of Professor Ana Margarida Madeira Viegas de Barros Timmons, Department of Chemistry, University of Aveiro and Professor Doutor Rui Ramos Ferreira e Silva, Department of Ceramics and Glass, University of Aveiro.

Dissertação de mestrado apresentada à Universidade de Aveiro para a exigência do cumprimento parcial do Mestrado em Ciência de Materiais, sob a supervisão da Professora Doutora Ana Margarida Madeira Viegas de Barros Timmons, Departamento de Química, Universidade de Aveiro e do Professor Doutor Rui Ramos Ferreira e Silva, do Departamento de Cerâmica e do Vidro, Universidade de Aveiro.

Financially supported by the European commission through the Erasmus Mundus Scholarship scheme.

O júri

Presidente

Doutor Paulo Jorge Almeida Ribeiro Claro

Professor Associado da Universidade de Aveiro

Vogais

Doutora Ana Margarida Madeira de Barros Timmons

Professora auxiliar da Universidade de Aveiro

Professor, Dr.-Ing. Karl Schulte

Professor at the Technical University Hamburg-Harburg

Doutora Maria da Conceição de Jesus Reigo Paiva

Professora auxiliar da Universidade do Minho

Acknowledgements

It is a pleasure to take this opportunity and thank those people without whose support this thesis would have been impossible. First and for most, I would like to owe my deepest and sincere gratitude to my supervisor, Professor Ana Barros and co-supervisor Professor Rui Silva, whose encouragement, guidance, support and patience has enabled me progress in understanding the subject matter and in writing this thesis.

I am deeply grateful to Professor Antonio F. Cunha, Department of Physics, University of Aveiro, who has helped me in undergoing the plasma treatment and for the valuable discussions we had throughout my experimental work. My warmest thank is due to Diogo Mata and Dr. Filipe Oliveira who made themselves available in preparing the vertically aligned carbon nanotubes and carrying of the compression tests, respectively. I am also very thankful to Celeste Azevedo, who has helped me in the analysis of my samples using the FTIR Spectrophotometer, Marta Ferro, who has helped me in acquiring SEM and TEM images and Tozé Fernandes, who has helped me in carrying out the Raman Study. I want to extend my sincere regards to Belinda Soares and Ana Caço who have helped me untirelessly in finding out supplementary materials during the experimental work.

I wish to thank my family for their encouragement and support. Their advices were truly helpful in time of difficulties.

It is an honor to thank the European Commission for their generous scholarship in financing my master's degree study, i.e. European Masters in Materials Science (EMMS), through the Erasmus Mundus scholarship scheme.

Last but indeed not the least; I exalt God for maintaining and strengthening me through the tests in life.

Keywords ATRP polymerization; Plasma treatment; VACNT; Zipping effect; Compressive strength

Abstract

Vertically aligned carbon nanotubes (VACNT) were synthesized using thermal chemical vapour deposition (CVD) technique and modified with oxygen-containing functional groups (hydroxyl, carbonyl and carboxyl) using an $Ar:O_2$ (97:3) plasma. X-ray photoelectron spectroscopy (XPS), Raman spectroscopy and scanning electron microscopy (SEM) have confirmed that those functional groups have been successfully grafted from the surface of the nanotubes. The plasma treatment was also found to remove significant amounts of amorphous carbon produced and deposited on the forests during the CVD process.

The aligned carbon nanotube forests were further modified with an atom transfer radical polymerization (ATRP) initiator to grow poly(methyl methacrylate) (PMMA) chains *via* an *in situ* controlled/living radical polymerization. The resulting VACNT/PMMA composite was analyzed using Raman, Fourier transform infrared (FT-IR) and proton nuclear magnetic resonance (^{1}H-NMR) spectroscopies, and scanning transmission electron microscopy (STEM). The TEM image mode and the ^{1}H-NMR results clearly showed the presence of a polymer matrix surrounding the vertically aligned CNT forests. In addition, compressive tests carried out for both pristine VACNT and VACNT/PMMA composite have showed a higher compressive strength of the composite material than the pristine. This resulted from the denser structural arrangement of the vertically aligned CNTs due to the zipping effect observed for CNTs in solution processing methods and due to the presence of the polymer matrix, which gives extra support for the VACNTs.

Palavras-Chave Polimerização por ATRP, Tratamento com plasma; VACNT; Efeito *Zipping*; Resistência à compressão

Resumo

Nanotubos de carbono alinhados verticalmente (VACNT) foram preparadas por deposição química em fase vapor (CVD) em parede quente e posteriormente submetidos a um tratamento com plasma de uma mistura Ar:O_2 (97:3) de modo a obter grupos hidroxilo, carbonilo, carboxílo à superfície. Esta modificação superficial dos nanotubos foi confirmada através das espectroscopias de XPS e de Raman, bem como por microscopia electrónica de varrimento. Os resultados obtidos mostraram ainda que através do tratamento de plasma se remove uma quantidade significativa de material grafítico que fora depositado durante o processo CVD.

Após o tratamento com plasma dos VACNT, procedeu-se ao ancoramentp do iniciador de polimerização radicalar por transferência e átomo (ATRP) à sua superfície. Seguidamente procedeu-se à preparação de cadeias de poli(metacrilato de metido) (PMMA) a partir da superfície. O compósito obtido VACNT/PMMA foi caracterizado pelas espectroscopias de Raman, de FT-IR e 1H-RMN e ainda por microscopia de transmissão electrónica em varrimento (STEM). Os resultados obtidos a partir de imagens em modo TEM e do RMN-1H confirmaram a presença da matriz polimérica em torno dos VACNT. Além disso, os testes de compressão realizados tanto para as florestas originais, como para o compósito, revelaram que este último apresentou uma resistência à compressão superior que resulta da compactação (*zipping*) sofrida pelos tubos durante o processamento em solução, bem como da presença da matriz polimérica a qual confere uma maior estabilidade dimensional e mecânica à floresta de CNTs.

Table of Contents

List of figures viii

List of Tables x

Abbreviations and Acronyms xi

1. Introduction 1

1.1. Motivation 2

2. Literature review 5

2.1. Structure and types of CNTs 5

2.2. Properties of CNTs 8

2.2.1. Chemical and physical properties 8

2.2.2. Electronic properties 8

2.2.3. Optical properties 9

2.2.4. Mechanical properties 9

2.2.5. Thermal properties 10

2.3. Synthesis methods of CNTs 11

2.3.1. Electric-arc discharge 11

2.3.2. Laser ablation 12

2.3.3. Chemical vapor deposition (CVD) 12

2.4. Synthesis of vertically aligned CNTs (VACNTs) 13

2.5. Surface modification of CNTs 15

2.5.1. Covalent modification method 15

2.5.2. Non-covalent functionalization 20

2.6. Polymer composites based on VACNTs *via* ATRP 20

3. Experimental 23

3.1. Chemicals 23

3.2. Instruments 23

3.3. Procedures 24

3.3.1. Synthesis of VACNT 24

3.3.2. Plasma treatment of the VACNTs 24

3.3.3. Grafting the ATRP initiator onto plasma treated VACNTs 24

3.3.4. ATRP polymerization of MMA from initiator-modified VACNTs 25
3.3.5. Preparation of blank PMMA 26

4. Results and discussions 27

4.1. Synthesis of VACNTs 27

4.2. Surface modification of VACNTs 29

4.2.1. X-ray photoelectron spectroscopy (XPS) analysis 31
4.2.2. Raman spectroscopy analysis 35
4.2.3. Morphological studies 40

4.3. ATRP polymerization of MMA from VACNT surface 42

4.3.1. Morphological studies 45
4.3.2. Fourier transform infrared spectroscopy (FTIR) analysis 51
4.3.3. Proton nuclear magnetic resonance (^{1}H-NMR) analysis 53
4.3.4. Miscellaneous comments on VACNT composites 55

4.4. Compression tests 57

5. Conclusions and recommendations 63

6. References 65

List of figures

Figure 1: An (8, 4) CNT formed by rolling a graphene sheet along the chiral vector C = $na_1 + ma_2$ where a_1 and a_2 are graphite lattice vectors. The nanotubes can also be characterized by the circumference, |C|, and the chiral angle, θ, with respect to the zigzag axis, $\theta=0^o$ [18]. 5

Figure 2: By rolling a graphene sheet in different directions the achiral, armchair (a) and zigzag (b), and the chiral (c) CNTs can be obtained [11, 22]. 6

Figure 3: Schematic representation of multi-walled (a) and single walled (b) carbon nanotubes [23]. 7

Figure 4: Schematic representation of typical CVD apparatus [12]. 13

Figure 5: Two types of growth mechanisms for acetylene based CVD (a) tip growth mechanism and (b) base growth mechanism [12]. 13

Figure 6: SEM image of aligned CNTs grown on glass substrate using PECVD [45]. 14

Figure 7: Photographic picture of millimeter size SWCNT forest prepared by super growth [11]. 14

Figure 8: Schematic presentation of various sidewall functionalizations of SWCNTs [47]. 16

Figure 9: Defect functionalization of CNTs by various functional groups using different chemical oxidation methods [47]. 18

Figure 10: Typical VACNT (~200 μm) used in our experiment produced by thermal CVD. 28

Figure 11: Mechanism for the formation of functional groups on the surface of CNTs through ozonlysis and radical reaction..... 31

Figure 12: XPS survey scan of (a) pristine and (b) plasma treated VACNTs. 32

Figure 13: Comparative presentation of (a) C 1s and (b) O 1s XPS spectra of pristine and plasma treated VACNTs, respectively. 33

Figure 14: Raman spectra of the pristine VACNT (a) and plasma treated VACNTs (b and c) at 20 W for 10 minutes and 2 W for 30 minutes, respectively. 37

Figure 15: The Raman spectra of pristine (a), plasma treated (b) and heat+plasma treated (c) VACNT samples. 38

Figure 16: SEM images of (a) pristine, (b) plasma treated, (c) heat+plasma treated, and (d) nitric acid treated VACNTs. 41

Figure 17: The mechanism of ATRP reaction. Note: P_n-X represents initiator grafted CNT [98]... 43

Figure 18: Reaction scheme of the ATRP polymerization of MMA from bromine-initiator-containing VACNT. 44

Figure 19: VACNTs/PMMA composites prepared using GO-modified (a, b) and CNF-modified (c, d), ATRP methods. The VACNTs were modified using an Ar/O_2 plasma at 20W for 10 minutes. 45

Figure 20: STEM image of pristine VACNT and VACNT/PMMA composite via CNF-modified method: (a) and (c) TEM and (b) and (d) SEM images..... 48
Figure 21: FTIR spectra of plasma treated VACNT (a), heat+plasma treated VACNT (b), PMMA grafted VACNT composite (c), and reference commercial PMMA (d) samples. Note: Although the FTIR spectrum of the blank PMMA prepared in our laboratory had shown more or less similar characteristic peaks as in the commercial PMMA, it is not presented here due to the presence of a significant amount of signal interference from water. 52
Figure 22: ^{1}H-NMR spectra of blank PMMA (a), which is plotted for comparison and that of VACNT/PMMA composites ^{1}H-NMR spectra prepared through GO-modified method (b) and CNF-modified method (c). 55
Figure 23: 5 mm×10 mm of the free standing VACNT/PMMA composite removed from the surface of the substrate prepared through CNF-modified method. 56
Figure 24: Schematic representation of compressive test for VACNT. (a) Free standing before compression, (b) buckled during compression and (c) springing back of VACNTs after compression [108]. 58
Figure 25: Compressive standard force vs compressive displacement of pristine VACNT/PMMA composite (a) and pristine VACNT (b). 60

List of Tables

Table 1: Summarized properties of single-walled, multiwalled and vertically aligned CNTs..... 11

Table 2: Elemental compositions and oxygen to carbon ratio (in at %) of pristine and plasma treated VACNTs..... 34

Table 3: The area ratios of the D-band to the G-band of the pristine, 2 W for 30 minutes and 20 W for 10 minutes oxygen plasma treated VACNTs..... 37

Table 4:The intensity ratios of D-band to G-band of the pristine, heat+plasma treated and plasma treated VACNTs..... 39

Abbreviations and Acronyms

AFM	Atomic force microscope
ATRP	Atom transfer radical polymerization
CNT	Carbon nanotubes
CVD	Chemical vapor deposition
GPC	Gel permeation chromatography
HiPCO	High pressure carbon monoxide
iCVD	Initiated chemical vapor deposition
MWCNT	Multiwall carbon nanotubes
^{1}H-NMR	Proton nuclear magnetic resonance
PE-CVD	Plasma enhanced-chemical vapor deposition
PMMA	Polymethyl methacrylate
RBM	Radial breath mode
SEM	Scanning electron microscope
STEM	Scanning-transmission electron microscope
SWCNT	Single wall carbon nanotubes
TEM	Transmission electron microscope
TMA	Thermo-Mechanical Analysis
VACNT	Vertically aligned carbon nanotubes
VARTM	Vacuum Assisted Resin Transfer Mold
VHS	Van Hove singularity
XPS	X-ray photoelectron spectroscopy

1. Introduction

Carbon nanotubes (CNTs) are one of the allotropic forms of carbon, which exist as a seamless, cylindrically rolled-up graphene sheets (planar-hexagonal arrangement of carbon atoms distributed in a honey comb lattice). They have a diameter in the range of nanometer, and their length can extend to more than a millimeter. Although carbon nanotubes had been recognized since the 1950s [1] as by-products from processes that produces carbon in its elemental form, such as arc discharge techniques and chemical vapor deposition (CVD), they were popularized and their potential significance was heralded only after the extensive study by Sumio Iijima in 1991 [2]. Primarily, he observed several concentric seamless cylinders of graphenes using TEM while studying on the by-products of fullerene synthesis by electric arc technique. These materials are known as multiwalled carbon nanotubes (MWCNTs). Two years later again himself and Bethune et al., independently reported single walled carbon nanotubes (SWCNTs), which consists in only a single wall of graphene seamless cylinder [3, 4]. Since the discovery of CNTs almost two decades ago, loads of articles, reviews and books have been published regarding their fundamental science and potential application areas [5-13].

As in graphene, bonding in CNTs is essentially sp^2. However, the circular curvature causes sigma-pi (σ-π) bonds rehybridization, where some sigma bonds are out of plane and π orbitals are more delocalized on the outer side of the tubes. Owing to these unique structural and electronic arrangements along with their one dimensional nature, CNTs are exciting materials with unique and extraordinary properties such as ballistic electrical [14] and high thermal conductivities [15] as well as superb mechanical properties unparalleled by any other materials. They are the stiffest and strongest materials ever known [16]. Their remarkable properties have led to potential and promising application areas such as reinforcing agents for high performance composites, field emitters for large area flat panel displays, energy storage devices, sensors, catalyst support, membranes, nanotools and nanoprobes (as tips for scanning tunneling, atomic force and magnetic force microscopes) and so on [5-7, 10-13]. However to utilize their unique properties in most of those listed applications, alignment of the CNTs is very essential. As a result CNTs are synthesized as vertical arrays (forests) on appropriate substrates.

Generally, CNTs can be produced by three main techniques: arc discharge, laser ablation and catalytic chemical vapor deposition (CVD). CVD is the most widely used synthesis method as a result of its simple and versatile processing conditions involving relatively low temperature and low cost. Moreover, being very easy to scale-up for industrial-scale CNTs production has also an important contribution for its popularity. It is also the only suitable method for the preparation of vertically aligned carbon nanotubes (VACNTs). Essentially, the CVD method consists of two steps. First transition metals (Fe, Ni or Co) catalysts are deposited on substrates and then the nanotubes are grown from the metal catalyst. The CNTs could grow vertically more than hundreds of a millimeter as a result of the catalyst density and the van der Waals forces that hold them together. The organization and morphology of the synthesized millimeter long, large block VACNTs would enable the enhanced utilization of their spectacular properties for various potential applications.

For instance, their high surface area to volume ratio and chemical inertness makes them an attractive candidate as fuel cell electrodes, supercapacitors, electromechanical switch devices and catalyst support [10, 17]. Furthermore, due to their nanometer-range diameter and high aspect ratio, they can be used as field emission electron source in the cathode of electron microscopes, flat panel displays, cathode ray tubes, lighting elements and vacuum power switches [7, 10 and 18]. Polymers films reinforced with aligned CNTs can find application as a mechanical damping in cars and aircrafts. The high compressibility of VACNTs would also allow building electromechanical pressure sensors [19]. Membrane filters made from VACNTs could be used for selective transport of species, which could find applications in water purification [7, 20]. Another possibility for the use VACNTs is as dry adhesives and super-hydrophobic surfaces. A study has showed that properly engineered VACNTs could have better adhesive effect than gecko feet [21].

1.1. Motivation

For more than a decade CNTs have received significant attention from the scientific community and there are still a lot of efforts going on everywhere to introduce them into the consumer market in large quantities. However, real issues associated with controlled synthesis, processability, manipulation and integration into conventional technologies have hampered to do so. In fact, from the very beginning, it has been realized that CNTs are inhomogeneous materials with different diameters, length and structure. They are also

insoluble in almost all solvents due to their strong van der Waals interactions as a result they are not easily processable. To integrate them into devices and composites, issues associated with homogeneity, alignment and processability have to be addressed. At least, by using vertically aligned CNTs issues associated with alignment can be solved. However, the processability of VACNTs is much worse than non-aligned CNTs. In part this is attributed to their alignment itself. Since the CNTs are grown on a substrate, it is very difficult to undergo various chemical modifications maintaining their alignment. And processing them in solution could also lead to the loss of their vertical alignment due to collapse. In addition, they are very weakly bound on the surface of the substrates and can be easily damaged even with a slight touch of a tweezers.

Bearing the above issues into mind, this work focuses on the following main themes:

a. To use vertically aligned CNTs produced by thermal CVD to overcome issues associated with alignment.
b. Carrying out an argon/oxygen plasma treatment on VACNTs to modify their surface by attaching oxygen containing functional groups to prepare them for grafting an ATRP initiator.
c. Study the feasibility of using an *in situ* atom transfer radical polymerization (ATRP) to grow poly (methyl methacrylate) chains from the surface of VACNTs.
d. Characterization of the reinforced composites using FTIR, Raman, ^{1}H-NMR, XPS and STEM.
e. Study the robustness of the reinforced VACNTs composite with a polymer matrix by undergoing compressive test and study its potential applications.

This thesis is organized as follows: first, following the general overview of CNTs (including vertically aligned CNTs) and their potential applications in the introduction part, an expanded view of CNTs regarding their structure, properties, synthesis and modifications methods are presented in the literature review. Moreover, the preparation of polymeric composites based on an *in situ* living radical polymerization, i.e. ATRP is discussed. The subsequent sections are devoted to the experimental and results and discussion parts. In these sections the preparation of VACNTs using thermal CVD along with an argon/oxygen plasma treatment for their surface modification and ATRP

polymerization for grafting PMMA chains from the surface of VACNTs are studied. And also the compressive property of the prepared VACNT/PMMA composite material is tested by undergoing compressive measurement. In the final sections, conclusions and recommendations are presented based on the analysis from the previous sections.

2. Literature review

2.1. Structure and types of CNTs

As described in the introduction part, CNTs are hollow, cylinder-like structures formed by rolling-up graphene sheets and whose ends are closed by a hemispherical-fullerinic cap. Interestingly, the way these graphene sheets are rolled-up can produce different kinds of nanotubes with different curvature, diameter and wrapping angle (helicity). In principle, any vector, **C**, connecting two crystallographically equivalent points in the graphene sheet can be joined (figure 1). This vector, **C**, is expressed as a linear combination of graphene lattice vectors $\boldsymbol{a_1}$ and $\boldsymbol{a_2}$ as expressed in (1).

$$\boldsymbol{C} = n\boldsymbol{a_1} + m\boldsymbol{a_2} \quad (1)$$

Where, *n* and *m* are integers that denote the tube as (*n*, *m*).

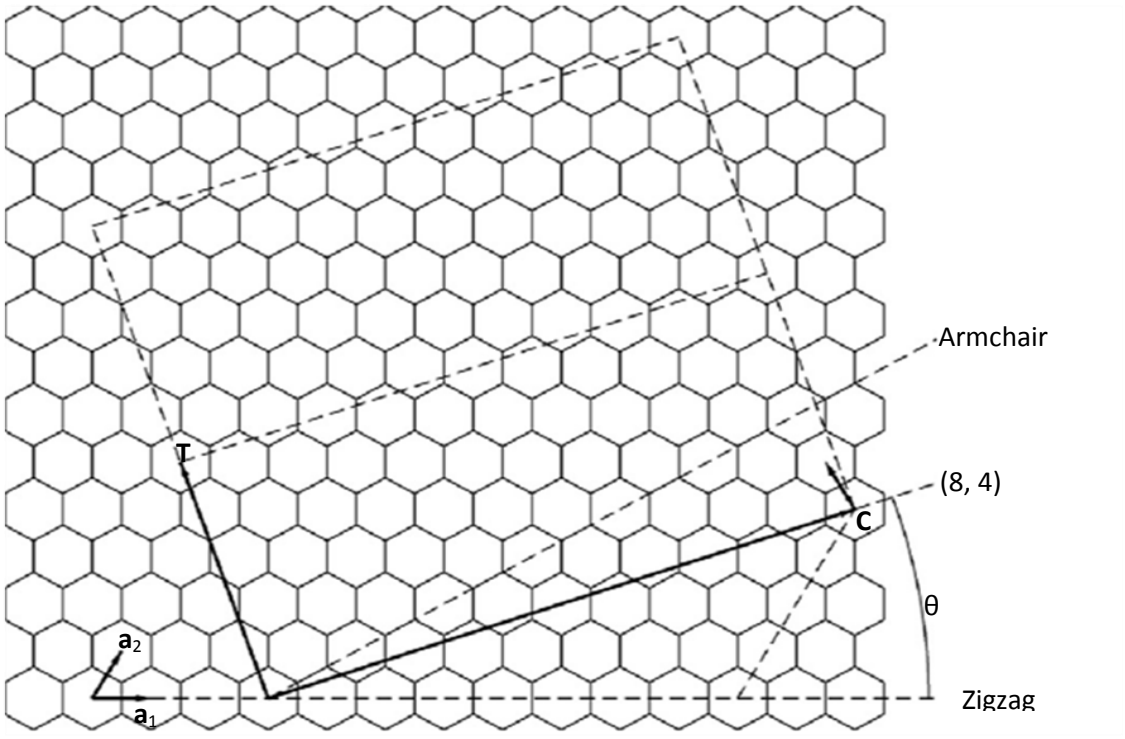

Figure 1: An (8, 4) CNT formed by rolling a graphene sheet along the chiral vector C = $n\mathrm{a}_1 + m\mathrm{a}_2$ where a_1 and a_2 are graphite lattice vectors. The nanotubes can also be characterized by the circumference, |C|, and the chiral angle, θ, with respect to the zigzag axis, $\theta=0^{o}$ [18].

Furthermore, the orientation of the graphene lattice to the cylinder axis are also determined by the two integers "*n*" and "*m*", which defines the chirality or helicity of the nanotubes. Based on their chirality two types of CNTs can be named: achiral and chiral. Achiral CNTs consist in the armchair (n, n) and zigzag (n, 0) types of CNTs whereas the remaining ones are chiral (figure 2). Chiral nanotubes are defined by the chiral angle, θ, which is defined as the angle between the vector $\boldsymbol{C}$, and the zigzag direction $\boldsymbol{a_1}$ shown in figure 1. Their chiral angle is calculated by the equation given in (2):

$$\theta = \tan^{-1}\left[\frac{\sqrt{3}m}{(m+2n)}\right] \qquad (2)$$

And their diameter is given by:

$$D = \frac{|\mathbf{C}|}{\pi} = a\frac{\sqrt{(n^2 + nm + m^2)}}{\pi} \qquad (3)$$

Where the lattice constant $a = |\boldsymbol{a_1}| = |\boldsymbol{a_2}|$

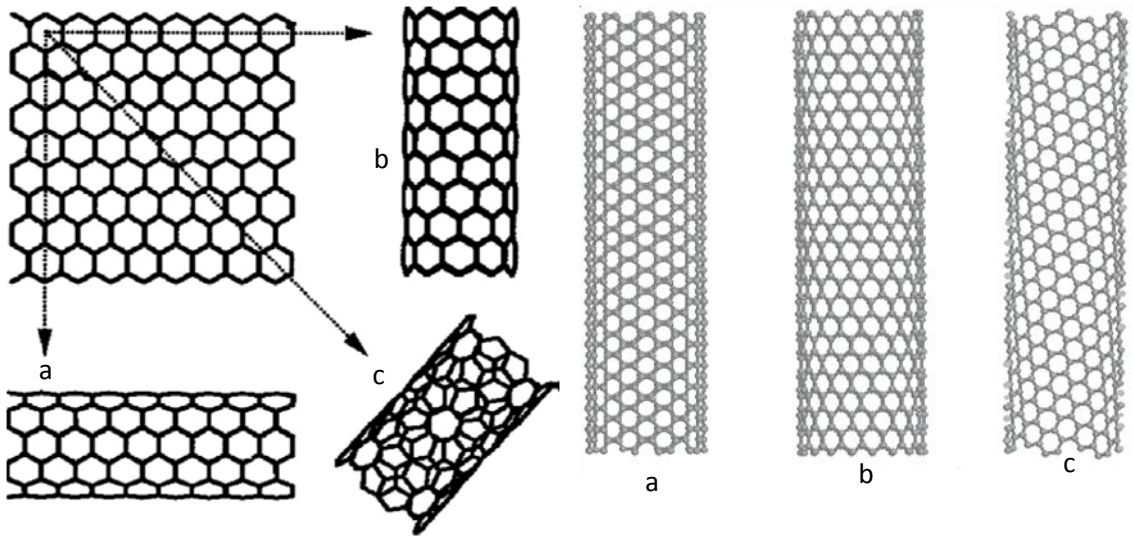

Figure 2: By rolling a graphene sheet in different directions the achiral, armchair (a) and zigzag (b), and the chiral (c) CNTs can be obtained [11, 22].

Based only on their diameter and chirality, CNTs can be either metalllic or semiconducting, with band gaps that are relatively large (≈0.5 eV) or small (≈10meV), respectively. For similar chirality and semiconducting CNTs, the band gap is inversely proportional to the diameter. Thus, there are infinite possibilities in the type of CNT molecules produced, and each could exhibit distinct physical properties [22, 23].

Broadly, depending on the number of concentric nanotubes, they can also be categorized into two groups as single walled carbon nanotubes (SWCNT) and multi-walled carbon nanotubes (MWCNT) (figure 3). The basic structure of both SWCNTs and MWCNTs are derived from the planar graphene sheets shown in figure 1. SWCNTs contain only a single hollow cylindrical wall of CNT whereas MWCNTs contain two or more concentric cylindrical walls of CNTs.

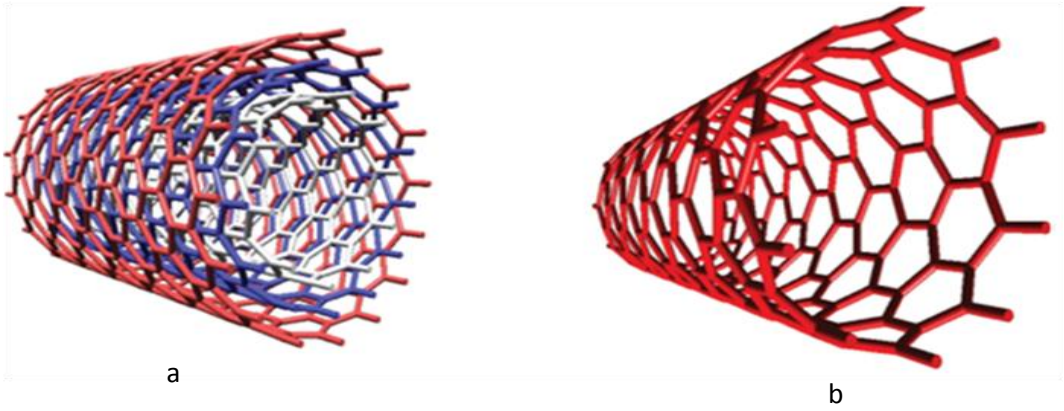

Figure 3: Schematic representation of multi-walled (a) and single walled (b) carbon nanotubes [23].

CNTs can assume different diameters; however, typical diameters for SWCNTs are in the range of 0.6 to 2.0 nm. It is unlikely to get an isolated nanotube with a diameter less than 0.4 nm as there is a limit associated with the strain developing as a result of wrapping graphene sheets into cylindrical structure. Larger diameter CNTs, above 3.0 nm, are also less stable as they tend to collapse unless supported by external forces or concentrically surrounded by neighboring CNTs, as in MWCNTs. The smallest innermost nanotube in MWCNT was found to be as small as 0.4 nm whereas the outermost tube can be as large as hundreds of nanometer. But typical values are larger than 2 nm inside and smaller than 100 nm outside. Moreover, the intertube distance between the concentric cylinders in MWCNT has a value of 0.34 nm [8, 11].

For vertically aligned CNTs the diameter and the number of walls of the nanotubes are dependent on various factors such as the size of the metal catalyst and support, and the flow of the carbonaceous feedstock used in the CVD. For example, for 1 nm Fe catalyst and 10 nm Al_2O_3 support, SWCNT of diameter 1-3 nm as well as DWCNT of diameter 5 nm are produced [24, 25].

2.2. Properties of CNTs

CNTs have similar bonding and structure as graphene. However, the circular curvature in CNT causes some of the sigma (σ) bonds to be out of the plane and the pi (π) orbitals become more delocalized on the outer side of the tubes due to the σ-π rehybridization. As a result, the nanotubes become mechanically stronger, thermally and electrically more conductive, and chemically and biologically more active than graphenes [10]. Their physical, chemical and mechanical properties also vary drastically based on the type (SWCNT, MWCNT), chirality (chiral, achiral), alignment and presence or absence of defects [11, 16].

2.2.1. Chemical and physical properties

Except in certain organic solvents like toluene, dimethylformamide (DMF) and tetrahydrofuran (THF), where CNTs can be made to form stable suspensions, they are very difficult to disperse in almost all kinds of solvents due to the strong van der Waals forces that hold them tight together to form bundles [9]. They are also extremely resistant to wetting Therefore, chemical functionalization by polar groups is essential to enhance their solubility and processability. This can be achieved by treating them with strong acids such as nitric and sulfuric acid, chemical oxidizers such as potassium permanganate and ozone or by treating them with various kinds of plasma. Usually, the end caps are more susceptible and easily functionalized than the sidewalls to these treatments due to the strain associated in their pentagonal or heptagonal structure. Yet, the sidewalls could also be functionalized albeit their chemical stability rendered by the graphitic structure. More detailed account regarding surface functionalization will be offered in section 2.5.

2.2.2. Electronic properties

The electronic properties of CNTs are sensitive to their geometric structure (chirality and diameter). Based on their chirality, CNTs can be metallic or semiconducting. Metallic conductance occurs when the following equation is satisfied:

$$(n-m)=3q \tag{4}$$

where q is an integer and n and m are the parameters mentioned in (1). For q=0, the nanotubes are reported to be metallic [11]. This suggests one third of the nanotubes i.e. armchairs (n, n), to be metallic and the remaining two thirds to be semi-conducting.

The band gap, E_g, for a particular semiconducting CNT with diameter D can be calculated using equation (5). Where d_{cc} is interatomic distance (0.144 nm for carbon) and γ is the interaction energy between the nearest neighbors.

$$E_g = \frac{2d_{cc}\gamma}{D} \tag{5}$$

CNTs have a unique electrical conductivity behavior than other electrically conducting materials. In metallic SWCNTs, for instance, the conduction of charge carriers is reported to be ballistic as a result of the reduced scattering [14]. As a result, they can sustain current densities up to 10^9 A/cm^2 without being damaged. This is about three orders of magnitude higher than copper wire [26]. Besides, MWCNTs with interconnected inner shells have even a better superconductivity behavior than SWCNT due to the intershell effect [27].

2.2.3. Optical properties

Defect-free and isolated CNTs, especially SWCNTs, offer a direct and well-defined band gaps, which is ideal for optical and optoelectronic applications. Normally, optical transitions occur when electrons or holes are excited from one energy level to another. Due to the one dimensional nature of CNTs, their electronic transitions give rise to peak energy band structures. These bands are known as van Hove singularities (VHS). Typically, the VHS of CNTs fall in the energy range of visible light. As a result visible light is strongly absorbed and they appear black. In addition to this CNTs are also reported to fluoresce in the near infra-red region [28].

2.2.4. Mechanical properties

The strongest bond in nature is the C-C sigma bond, which is present in materials like diamond and graphite. CNTs are also made of this type of bond, as a result they are as stiff as or even stiffer than diamond with the highest values of Young´s modulus and tensile strength. Although the direct measurement of their Young´s modulus is challenging, it can be inferred from atomic force microscopy (AFM) test. Most theoretical and experimental measurements on the elastic modulus of SWCNTs are reported to be in the range of 1 TPa-

1.3 TPa making them the stiffest materials known [11, 29]. For MWCNTs, where the individual CNTs are arranged concentrically, the Young´s modulus can even be higher than SWCNT due to contributions from coaxial inter-tube couplings and van der Waals forces. Nanoindentation tests carried out on VACNTs samples revealed that the effective bending modulus (E_t^b) and effective axial modulus (E_t^a) of MWCNTs to be in the range of 0.91-1.24 TPa and 0.90-1.23 TPa [30]. In spite of the fact that Young´s modulus is independent of tube chirality, it is dependent on tube diameter. Hence, the highest Young´s modulus values are obtained for CNTs in the diameter range between 1 and 2 nm.

The elastic response of CNTs to deformation is also superior. Most hard materials fail within a tensile strain of 1% or less due to the propagation of dislocations and defects but CNTs can sustain up to 15% tensile strain before fracture [5]. Likewise, the tensile strength of individual CNTs can also be as high as 150 GPa, which is two orders higher than steel.

2.2.5. Thermal properties

Unlike metals where heat is directly carried by electrons, in CNTs heat is almost exclusively transported through lattice vibrations known as phonons. The outstanding thermal conductivity of CNTs is related to the stiffness of the carbon-carbon covalent bonds. Theoretical calculations and experimental measurements showed that the thermal conductivity for a SWCNT ropes and MWCNTs at room temperature could vary between 1800 and 6600 $Wm^{-1}K^{-1}$ [31, 32]. At room temperature typical thermal conductivity value of 3500 $Wm^{-1}K^{-1}$ was reported for SWCNTs whereas for MWCNTs more than 3000 $Wm^{-1}K^{-1}$ was measured [33]. On the other hand, for large arrays of CNTs, the thermal conductivity is observed to be only 200 $Wm^{-1}K^{-1}$, lower by orders of magnitude from both MWCNTs and SWCNTs. Uncontrollable defects, build up of amorphous carbon during growth by CVD and thermal resistance created by tube-tube interaction are claimed to be responsible for this drastic drop [34].

Correspondingly, CNTs have also excellent thermal stability in inert atmosphere. They can be routinely annealed up to 1200 ^oC. Still they can also be annealed up to 1500 ^oC without causing significant damage. However, in air they burn in the range of 450-620 ^oC [9].

For a better and easier comparison, the properties of single-walled, mutliwalled and vertically aligned CNTs are tabulated in table 1.

Table 1: Summarized properties of single-walled, multiwalled and vertically aligned CNTs.

	SWCNT	MWCNT	VACNT
Diameter	0.6-2.0 nm	>0.4 nm (inside), <100 nm(outside)	0.5-250 nm
Length	100 nm-18.5 cm	100 nm-20 cm	up to 20 cm
Intrinsic band gap (metallic/semi-conducting)	0 eV/~0.5 eV	idem	idem
Current density	10^{7}-10^{9} A cm^{-2}	idem	-
Young´s modulus	1.05 TPa	1.20 TPa	0.9-1.23 TPa
Tensile strength	75 GPa	~150 GPa	-
Thermal conductivity	3500 $Wm^{-1}K^{-1}$	3000 $Wm^{-1}K^{-1}$	200 $Wm^{-1}K^{-1}$

2.3. Synthesis methods of CNTs

There are several methods to synthesize carbon nanotubes. Generally, the syntheses methods can be classified into two main categories based on the operating temperatures. The first one is a high-temperature route based on vaporization of a graphite target, which consists in an electric-arc discharge and laser ablation methods. The second way is a medium-temperature route based on catalytic chemical vapor deposition (CCVD), which consists in various kinds of CVD techniques such as thermal CVD and plasma-enhanced CVD. The high-temperature route leads to a high quality product with fewer structural defects as a result of high-temperature growth process that ensures perfect annealing of defects.

2.3.1. Electric-arc discharge

The fortunate discovery of MWCNTs was made in materials produced by the arc discharge process. The process involves vaporization of the graphite anode in a reduced atmosphere or inert gases (He, Ar) at a temperature >3200 ^{o}C (sublimation point of graphite) and condensing the resulting vapor under a high temperature gradient [10, 16]. The vapors are deposited as amorphous carbon, graphitic nanoparticles, fullerene and MWCNT. SWCNTs could be prepared if metal catalysts (Co, Ni, Fe, Y or Gd) are alloyed with the anode.

2.3.2. Laser ablation

The laser ablation technique is rather similar to the arc method. The apparatus contains a tube furnace maintained around 1200 ^{o}C under argon atmosphere and a high power laser source. The laser ablates a solid target of graphite (or graphite and metal catalyst for SWCNT) and the vapor is carried by gently flowing gas through a quartz tube into a high temperature oven (800 ^{o}C), where the product is collected [10, 16].

2.3.3. Chemical vapor deposition (CVD)

Although carbon nanotubes produced by the arc discharge and laser ablation methods have the highest quality (high crystallinity and low defect concentration), they are less amenable to scale-up for large quantity production of CNTs due to large amount of energy consumption. On the other hand, CVD technique is not only affordable but also allows more control over the growth process and purity at a relatively mild temperature conditions (≤1000 ^{o}C). In addition, it also yields high quantity CNTs in short time. The main drawback of CVD method is that the graphene structure is less defined [35]. However, this problem can be tackled by annealing the nanotubes between 1800-2600 ^{o}C under inert atmosphere [36].

The synthesis of carbon nanotubes by CVD involves the dissociation of a gaseous or volatile carbon feedstock such as methane, ethylene and acetylene in the presence of a nano-particle metal catalyst (mostly iron supported by alumina), which acts as a nucleus for the growth of the CNTs on a substrate (silicon or quartz). The synthesis is carried out in the temperature range of 600-1000 ^{o}C [35].

Based on the heat source used, CVD techniques can be categorized into two groups: thermal CVD and plasma enhanced CVD [11].

2.3.3.1. Thermal CVD

When a conventional heating source is used, such as resistive or inductive heater, furnace or IR lamps, the technique is called thermal CVD. The most promising ones in this category are: methane CVD [37, 38], alcohol CVD [39] and HiPCO, (high pressure catalytic decomposition of carbon monoxide) [40] A typical thermal CVD apparatus is shown in figure 4.

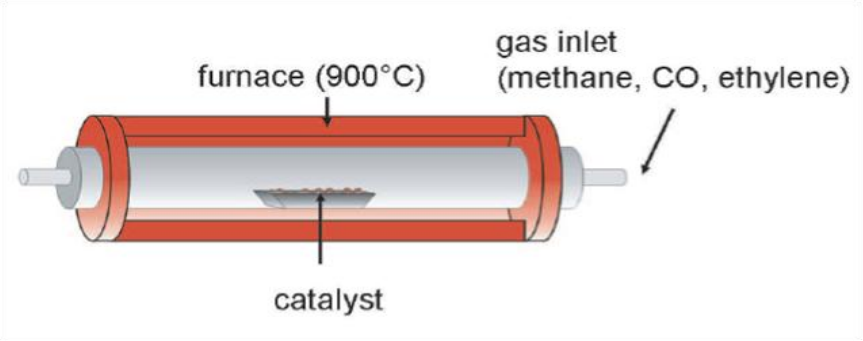

Figure 4: Schematic representation of typical CVD apparatus [12].

2.3.3.2. Plasma enhanced- CVD (PECVD)

PECVD is another variation of CVD where the heat source comes from plasma. This method yields high quality CNTs. Furthermore, the plasma has an extra advantage in controlling the diameter of the CNTs and selectively etches metallic SWCNTs [41].

2.4. Synthesis of vertically aligned CNTs (VACNTs)

Since both arc discharge and laser ablation techniques produce CNTs only in a rope or tangled form, CVD techniques have been the best route to produce vertically aligned CNTs. The vertical alignment in CVD process is achieved by self-assembly of the nanotubes into a vertical array. In addition to gain more rigidity, the nanotubes interact with each other *via* van der Waals. The growth mechanisms by which CNTs grow on a substrate are illustrated in figure 5.

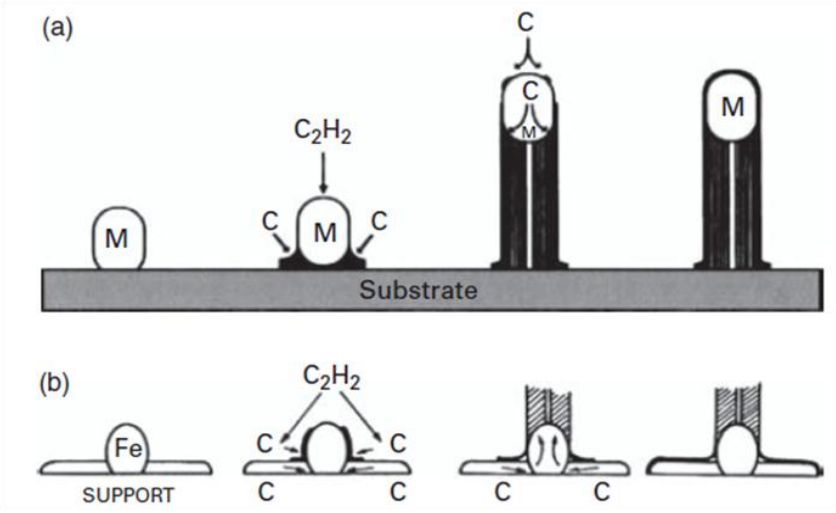

Figure 5: Two types of growth mechanisms for acetylene based CVD (a) tip growth mechanism and (b) base growth mechanism [12].

Various authors [42-44] have reported the growth of CNTs using different methodologies. However, the first successful demonstration of vertically aligned growth was made by Ren and co-workers who have grown large diameter vertically aligned MWCNTs on a glass substrate by PECVD (figure 6) [45].

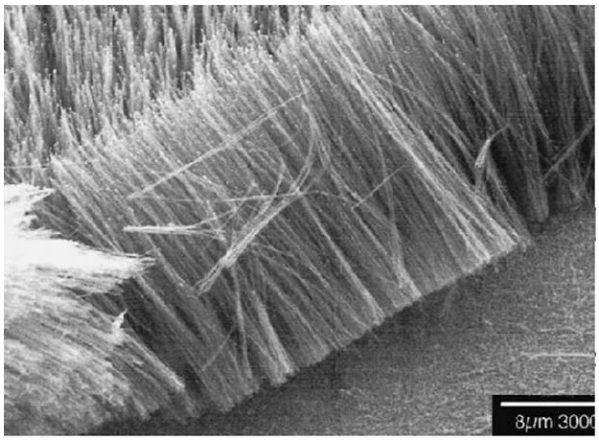

Figure 6: SEM image of aligned CNTs grown on glass substrate using PECVD [45].

Most growth methods based on CVD are seriously limited by the low activity and short life time of the catalyst. However, the addition of a small and controlled amount of water vapor during the growth process enhances the activity and lifetime of the catalyst resulting in very long VACNTs. This approach is called **super growth** [43, 46]. This method yields highly dense, ultra long and impurity-free vertically aligned CNTs, with height exceeding a millimeter. This is exemplified by the photographic picture of typical ultra long VACNTs shown in figure 7.

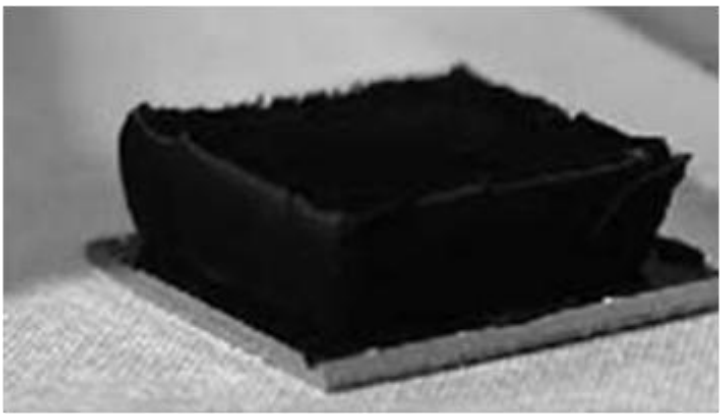

Figure 7: Photographic picture of millimeter size SWCNT forest prepared by super growth [11].

2.5. Surface modification of CNTs

CNTs are extremely resistant to wetting, and as a result it is very difficult to disperse them either in water or organic solvents. To benefit from their outstanding properties in various fields of application, it is necessary to modify their surface for an improved solubility and integration. Generally, there are two ways of modifying CNTs: covalent and non-covalent modification methods.

2.5.1. Covalent modification method

The covalent method modifies CNTs by attaching functional groups (carboxyl, hydroxyl, amine, etc.) on the carbon nanotubes scaffold through covalent bonding. In this process the sp^2 hybridized carbons are changed to sp^3 hybridization resulting in the loss of conjugation, which would compromise the electrical conductivity of CNTs. Despite this side effect, the attached groups have an important advantage of being derivatized so that they can be utilized to offset the low solubility and processability of CNTs in order to combine them with different materials including polymers.

There are two ways of modifying CNTs covalently. The first way operates by directly attaching groups to the surface of the CNTs. This is called sidewall functionalization. On the other hand the second one known as defect functionalization utilizes groups already bound on the nanotubes, derived from either intrinsic or induced defects, to modify their surfaces.

2.5.1.1. Sidewall functionalization

Functionalization of carbon nanotube sidewalls usually involves the direct treatment of pristine tubes with very reactive species such as halogens, carbenes, nitrenes or arynes. As in fullerenes, an increase in the curvature of the carbon shell increases the tendency to undergo addition reactions [47, 48]. It follows that smaller diameter nanotubes display an enhanced reactivity in comparison to larger diameter nanotubes. In the schematic diagram shown in figure 8, various sidewall functionalization methods of SWNTs are depicted.

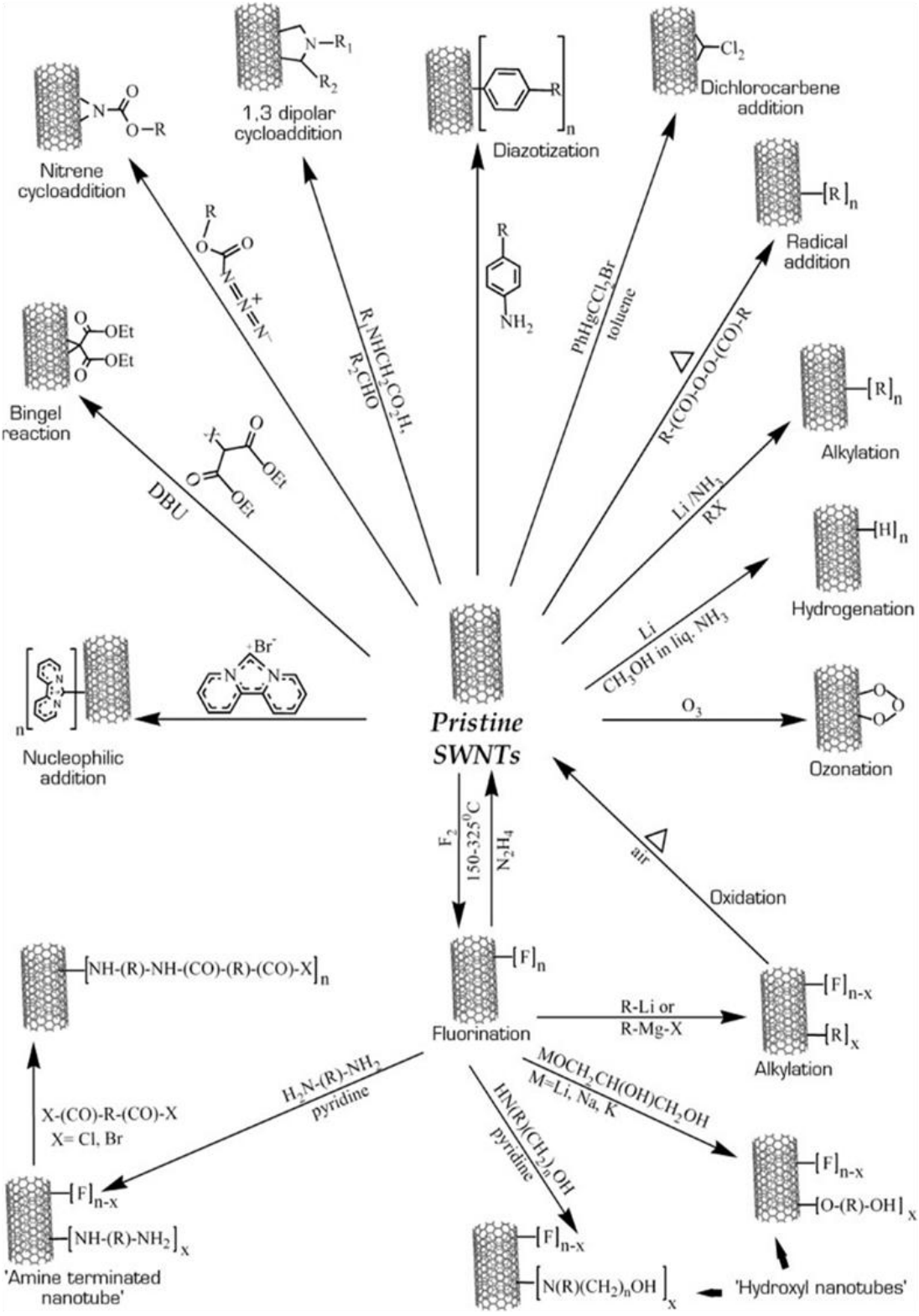

Figure 8: Schematic presentation of various sidewall functionalizations of SWCNTs [47].

In 1998, Mickelson et al. have reported one of the first sidewall functionalization of CNT using elemental fluorine [49]. Now, fluorinated CNTs are commercially available and have the advantage of being further derivatized using Grignard reagent or alkyl lithium reagents. At about the same time, Haddon et al. demonstrated the functionalization of CNT sidewalls using carbenes [50]. Although carbenes normally react with carbon double bonds by forming a cyclopropane ring, zwitterionic carbenes such as dipyridyl imidazolium carbene, can form a single covalent bond with CNTs. This method results in a product quite soluble in DMSO and with enhanced electrical property due to the presence of the zwitterions [51].

Radicals can also be grafted on CNTs electrochemically, photochemically or thermally. For example, Holzinger et al. have used photoinduced addition of perfluorinated radicals on CNTs [52]. Perhaps, the most notable technique to functionalize CNTs is by using the **Prato reaction** [53]. It follows a 1, 3-dipolar cycloaddition of azomethine ylides on CNTs, originally developed for the modification of fullerenes by Prato and coworkers [54]. The ylides are first prepared by the condensation of an α-amino acid and an aldehyde. Then, they are refluxed with CNTs to attach pyrollidine moieties on the surface of the nanotubes. This approach was found to work with both SWCNTs and MWCNTs.

The alkylation of CNTs was achieved by using alkyl lithium reagents. Viswanathan et al. have used *sec*-butyllithium reagent to create active anionic sites on the surface of SWCNTs for the polymerization of styrene by anionic polymerization process [55]. The carbanions created on the surface of the SWCNTs in addition to providing active sites for the attachment of polystyrene, they were also reported to serve as an exfoliating agent; i.e. they maintained the bundled CNTs apart. Another variation of the alkylation method was also reported by Liang et al. using lithium, in liquid ammonia followed by a reaction with alkyl halides for the sidewall functionalization of CNTs through alkyl radical intermediates [56]. The composite materials obtained from both these methods were soluble in common organic solvents such as chloroform, dimethylformamide and tetrahydrofuran.

Likewise, the covalent functionalization of VACNTs was demonstrated using several perfluoroarylazides as nitrene precursors in nitrene cycloaddition reaction. Then, the surfaces of the substrates that contain the aligned CNTs were used to prepare patterned superhydophilic regions on superhydrophobic surfaces [57].

2.5.1.2. End and defect functionalization

Defect functionalization takes advantage of defect sites created on the sidewalls or at the end caps of CNTs [48]. These defects are created either during the production process or during the oxidative purification process by HNO_3 [58], mixture of HNO_3 and H_2SO_4 [59], mixture of H_2SO_4 and H_2O_2 (Piranha) [60] or ozone [61]. They can be in the form of open ends and holes on the side walls or end caps terminated by oxygen containing functional groups such as carboxylic acid. These groups can be further modified to yield amides, esters and thiols through amidation, esterificaion, and thiolation, respectively (figure 9).

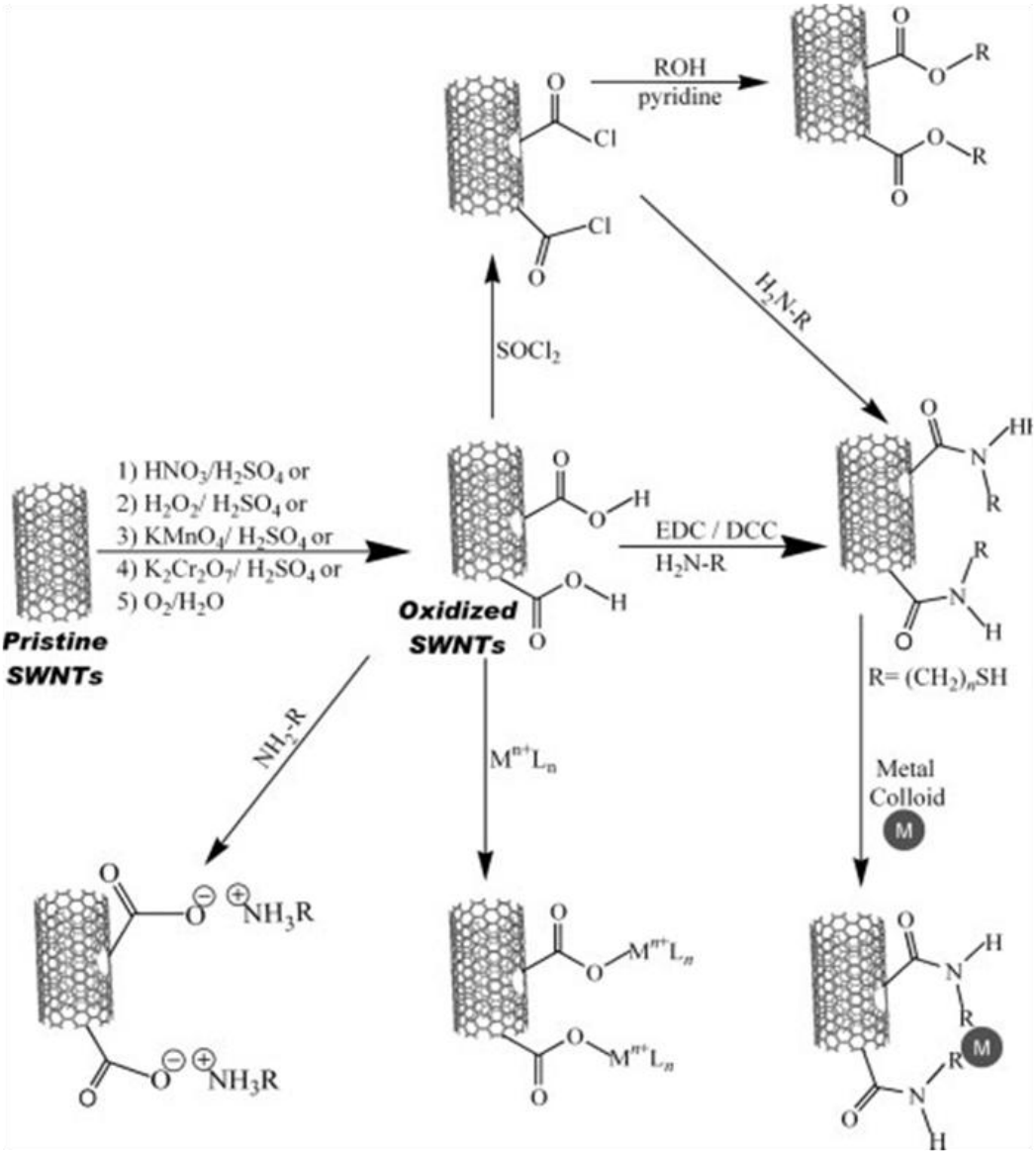

Figure 9: Defect functionalization of CNTs by various functional groups using different chemical oxidation methods [47].

Haddon et al. have reported the modification of SWCNT containing carboxyl acid functional groups by long chain alkyl amine (octadecylamine; ODA) through amidation [62]. The modified SWCNTs were reported to gain substantial solubility in chloroform, dichloromethane, carbon disulfide and most aromatic solvents. Replacing the ODA by octadecylalcohol has also resulted in a soluble ester functionalized SWCNT [63]. On the other hand, Kim et al. have succeeded in the thiolation of carboxylated CNTs using $NaBH_4$, $SOCl_2$, and Na_2S [64].

2.5.1.3. Electrochemical modification

Electrochemistry is a valuable tool that uses an applied potential to produce reactive species such as radicals for the functionalization of CNTs [48]. For example, electrochemical reduction of various aryl diazonium salts has been used to derivatize small diameter SWCNTs and carbon nanotubes derivatized with 4-*t*-butylbenzene moiety were found to possess significantly improved solubility in organic solvents [65].

Vertically aligned MWCNTs have also been functionalized using electrochemical method with molybdenum oxide (MoO_x) in Na_2MoO_4 solution. The MoO_x-modified VACNTs were reported to possess electrocatalytic ability towards the reduction of bromates [66]. In a similar manner, Ye et al. have also demonstrated the modification of VACNTs with platinum nanoparticles using electrochemical reduction method [67]. They have reported that the morphology of the VACNTs is retained after each electrochemical treatment using supercritical drying techniques.

2.5.1.4. Plasma modification

Plasma treatment is an alternative method of functionalizing materials surfaces including CNTs. It is an alternative approach to the conventional chemical modification methods as it allows environmentally friendly, less harsh and shorter reaction time to modify CNTs. Since no liquids are involved in this method, it overcomes the collapsing of VACNTs into mats observed during the wet chemical modification methods. The plasma is usually obtained by glow discharge when gases such as Ar, N_2, O_2 are exposed to a radio-frequency (rf) electromagnetic field at low pressure.

Plasma has been widely used for surface cleaning, surface activation and sterilization of materials. For instance H_2O- and O_2-plasmas have been successfully used to etch

amorphous carbon from aligned CNTs produced by CVD methods [68, 69]. Depending on the type of gases used in the plasma various types of functional groups can also be attached on the surface of CNTs.

The first instance on the plasma modification of CNTs was reported by Chen et al. [70]. They have used ethylenediamine- and acetaldehyde-plasma treated aligned CNTs to modify them with polysaccharides through Schiff base linkage.

Unlike the conventional chemical methods, the hydrogenation of CNTs was also achieved through plasma treatment. Cold ammonia plasma used by Khare et al. has functionalized SWNTs with hydrogen (–H) in addition to amine ($–NH_{2)}$ groups [71]. Vohrer et al. have used an argon/water/oxygen containing glow discharge plasma to generate polar groups such as alcohol, carbonyl and carboxyl moieties on CNTs and CNT sheets (bucky papers). They have also studied the influence of the plasma parameters such as power, pressure, treatment time, and process gases or gas mixtures on the amount and type of functional groups attached on the nanotubes [72, 73].

2.5.2. Non-covalent functionalization

Non-covalent functionalization is based on the ability of the extended π-system of the CNT sidewall to bind suitable molecules through π-π stacking or van der Waals interactions. The prospect of functionalizing the outer surface of CNTs in a non-covalent way is very attractive for electrical applications since the extended π-system would be undamaged. For instance, surfactants such as SDS [74], SDBS [75] and Triton X-100 [76] were shown to enhance the dispersion of CNTs in water without altering their electronic arrangement. Similarly, some polymers and small molecules containing planar groups are also used to modify the surface of CNTs in non-covalent way [77, 78].

2.6. Polymer composites based on VACNTs *via* ATRP

Since the first report on CNTs polymer composites by Ajayan et al. [79], the last one and half decade saw a plethora of papers published by various authors. However, factors such as entanglement, insolubility and difficulty in dispersing CNTs uniformly in the composites have hampered the successful utilization of their singular properties for developing outstanding materials. To address these issues different solutions have been

proposed. One of the solutions was to use vertically aligned CNTs for the preparation of composites by filling them with a polymer through adsorption or chemical bonding as VACNTs have an important advantage in solving issues associated with the alignment of nanotubes in composites.

ATRP is a controlled/living radical polymerization technique, which is one of the methods used for growing well-controlled molecular weight polymer chains from the surface of CNTs [80, 81]. Yao et al. adapted this polymerization technique for growing PMMA and P*t*BA polymeric chains from modified SWCNTs [82]. Initially, using 1, 3-dipolar cycloaddition reaction, they have introduced phenol groups on the surface of SWCNTs and then these groups have been reacted with 2-bromoisobutyrylbromide to modify their surface with an alkyl bromide moiety. They have used these modified-SWCNTs as macro-initiator for the ATRP polymerization of MMA and *t*BA. Similarly but using MWCNTs, ATRP of styrene and MMA have also been reported by Baskaran et al. [83]. Approximately 70 wt% of PMMA was found covalently grafted on the surface of MWCNTs whereas only 18 to 33 wt% was reported for polystyrene depending on the initiator concentration. This correlation between initiator concentrations on the nanotubes and the amount of polymer grafted on their surface, allowed the precise control of the molecular weight of the PMMA chains.

Of particular interest to our work, ATRP polymerization of initiator-modified vertically aligned CNTs with N-isopropyl acrylamide was reported by Sun et al. [84]. They oxidized CNTs using nitric acid and activated it with aminopropyltrimethoxysilane. Then, the initiator was anchored by reacting with bromoisobutyryl bromide. Eventually, a temperature responsive polymer poly(N-isopropyl acrylamide) [PNIPAAm] was grafted on the nanotubes through ATRP polymerization. Although CNT forests are known to collapse easily when they come in contact with liquid, they have reported that the aligned structure remain intact even after the polymerization process. They attributed this result to the high vacuum pre-treatment condition that strengthens the CNTs before the chemical oxidation.

Apart from grafting polymer chains from the surface of VACNTs oxidized by nitric acid, the grafting of PMMA and polystyrene (PS) chains from the surface of aligned MWCNTs using diazonium salt was reported by Matrab et al. for the first time [85]. To underway the reaction first they have grafted ATRP initiator (phenyl ethyl bromide) containing

diazonium salt onto the surface of the VACNTs using electrochemical method followed by an ATRP polymerization with MMA and styrene. The ATRP polymerization was demonstrated to be successful and the tethered polymer chains were observed forming dense organic adlayers over the surface of the VACNTs.

Pastine et al. have also demonstrated ATRP polymerization from aligned CNTs using Poly(N-isopropyl acrylamide) [57]. They have attached 2-bromoisobutyrate containing perfluoroazides on the surface of VACNTs using nitrene insertion method triggered by UV radiation. Then, the 2-bromoisobutyrate moiety served them as an initiator for the grafting of NIPAAm *via* ATRP. In addition with an appropriate photomask, they prepared patterned substrates with isolated polymerized features as small as 5 μm and a polymerized background with isolated pristine CNT regions as small as 60 μm.

3. Experimental

3.1. Chemicals

The list of chemical agents used consists in methyl methacrylate (MMA) (99%), 2-bromo-2-methylpropionylbromide (98%), ethylene-2-bromo isobutyrate (98%), N, N, N, N, N-pentamethyldiethylenetriamine (PMDETA) (99%), triethylamine (TEA) (99%) and tris(2-aminoethyl)amine, which were acquired from Aldrich (Sigma-Aldrich Chemicals SA). 4-Dimethylaminopyridine (DMAP) (99%) and $Cu(Br)_2$ were purchased from Fluka Chemicals. HPLC grade chloroform was purchased from Fischer Scientific. Ethanol absolute (99.5%) was purchased from Panreac Quimica (SAU). DMF (99%) was obtained from BDH^{TM} Laboratory Reagents.

3.2. Instruments

The IR spectra were acquired using a Bruker Tensor 27 FTIR spectrophotometer. The IR samples were prepared as a pellet using potassium bromide (KBr) and in some instances by applying chloroform-suspended CNT samples over sodium chloride (NaCl) window. The Raman spectra were obtained at room temperature in back scattering configuration with a Jobin-Yvon LabRam HR (λ=325nm) equipped with CCD detector. Bruker Avance 300 was used for recording the proton nuclear magnetic resonance (^{1}H-NMR) spectra of the blank and composite samples. The samples for the ^{1}H-NMR were first dispersed in deuterated chloroform inside an NMR tube and sonicated for 10 minutes prior to the measurement. The SEM and STEM images were obtained using a Hitachi Su-70 analytical Scanning Electron Microscope (Japan). For observing the VACNT samples under STEM, VACNT samples taken from the substrates were dispersed in ethanol by sonication and a standard TEM copper grid was immersed in the suspensions and left to dry in a desiccator. XPS measurements for the elemental and chemical bonding analysis were performed in a VG Scientific ESCALAB 200A spectrometer (in University of Porto) using non-monochromatised Al Kα radiation at 1486.6 eV. The XPS spectra were fitted using XPSPEAK 4.1. The compressive test was done using Zwick/Roell Z020 Universal testing machine with a load cell of 2 KN and maximum load of 30 N at a rate of 0.3 mm/min on a 10 mm by 3 mm substrate containing the pristine and polymer modified VACNTs.

3.3. Procedures

3.3.1. Synthesis of VACNT

The VACNTs were synthesized on a 1cm×1cm silicon substrate containing ~2 nm iron nanoparticles catalyst supported by ~10 nm alumina nanoparticles. The process involves the introduction of ethylene gas with a flow rate of 10 sccm and carrier gases, argon and hydrogen, at a flow rate of 400 and 100 sccm, respectively, into a thermal CVD reactor at a temperature of 750 ^{o}C. Within 10-30 minutes the VACNTs were obtained deposited on the silicon substrate.

3.3.2. Plasma treatment of the VACNTs

The plasma treatment was carried out in a vertically arranged plasma sputtering chamber. The copper cathode was covered by a plastic insulator to reduce contamination and the VACNTs samples were kept on top of the plastic covered cathode. Capacitatively coupled plasma from a radio frequency (rf) at 13.56 MHz was connected to the anode. And the cathode was grounded. The pressure inside the chamber was maintained at a pressure of ~0.1 mbar. Then a mixture of Ar:O_2 (97:3) gas was flown at 28 sccm into the chamber keeping the internal pressure more or less constant. The plasma treatment was carried out at loads of 20 W and 2 W for 10 and 30 minutes, respectively. These conditions were specifically chosen to maximize the yield of derivitizable groups such as hydroxyl, carboxyl and carbonyl groups on the surface of the VACNTs [73].

3.3.3. Grafting the ATRP initiator onto plasma treated VACNTs

Bromine-containing ATRP initiator was grafted onto the plasma treated surfaces of the VACNTs following the procedures reported in literatures [86] and [87], with only slight modifications, as outlined below.

a) **GO-modified method** [86]: A substrate containing plasma treated VACNT was loaded in a 100 mL round bottom flask containing DMF (15 mL). Triethylamine (TEA) (10mL) was added and tightly sealed using rubber septum. Then, the flask was purged by N_2 for 30 minutes and it was cooled in an ice bath. 2-bromo-2-methylpropionylbromide (15 mL) was added drop wisely for over 1 hour *via* syringe and the resulting solution was gently stirred for 24 hours at room temperature. The product was

decanted, and washed thoroughly with chloroform and distilled water. Finally, the initiator-modified VACNT product was kept to dry in a desiccator for 24 hours.

b) **CNF-modified method** [87]: A substrate containing plasma treated VACNTs was mixed with $CHCl_3$ (15 mL) in a 100 mL round-bottom flask equipped with a small magnetic stirrer and rubber septum. TEA (1 mL) and 4-dimethylaminopyridine (DMAP) (0.1 g) were added before purging the content in the flask with nitrogen for 30 minutes. Then, the solution was cooled in an ice bath. In a separate glass tube, sealed with a rubber stopper, ATRP initiator, 2-bromo-2-methylpropionylbromide (5 mL), was dissolved in chloroform (10 mL). Then, this solution was transferred drop by drop into the reaction flask over a period of 1 hour *via* syringe, followed by constant gentle stirring for 48 hours at room temperature. The resulting product was decanted and washed copiously with chloroform. The final product was collected after the sample was dried overnight in an oven at 40 ^{o}C.

3.3.4. ATRP polymerization of MMA from initiator-modified VACNTs

a) **GO-modified method** [86]: One piece of initiator grafted-VACNT substrate was added to a 50 mL round bottom flask containing of DMF (5 mL), MMA (5mL), tris(2-aminoethyl)amine (75 μL) and a small piece of copper(0) wire. The flask was sealed and degassed for 30 minutes. The mixture was, then, allowed to react at 80 ^{o}C for 18 hours using an oil bath. Ethanol (50 mL) was added to the resulting viscous solution to precipitate the product. Carefully, the substrate was decanted and washed three times with ethanol. Then, it was soaked in DMF (15 mL) and washed again with sufficient amount of ethanol to remove ungrafted monomers and excess reagents. Finally, the product was left to dry in an oven at 40 ^{o}C for 24 hours and kept in a desiccator.

b) **CNF-modified method** [87]: In a 100 mL round bottom flask containing DMF (6 mL), CuBr (38 mg), PMDETA (58 μL) and magnetic stirrer, initiator modified-VACNT were added and sealed with a rubber stopper. Then, the flask was degassed and refilled with nitrogen for 15 minutes. The monomer, MMA (5 mL) was taken *via* syringe and added into the reaction flask. The reaction mixture was stirred at 65 ^{o}C for 24 h using an oil bath. Then, the product was diluted with chloroform and decanted. The decanted product was further washed thoroughly with ample amount of chloroform to ensure total removal of ungrafted monomer and other reactants. Finally, the product was dried overnight in an oven at 40 ^{o}C and kept in a desiccator.

3.3.5. Preparation of blank PMMA

DMF (1mL), Cu(I)Br (15.7mg) and PMDETA (20μl) were mixed in a two necked flask equipped with a magnetic stirrer and sealed with a rubber stopper. The flask was flushed with nitrogen for 1 hour. In a separate glass tube, MMA (2 ml) was sealed with a rubber stopper and flushed with nitrogen for 30 minutes. The content from the glass tube and ethylene-2-bromoisobutrate (16 μl) were poured in the two neck flask, consecutively. Then, the mixture was reacted at 60 ^{o}C for 20 hours using an oil bath under constant stirring. Later on, the color of the solution was changed from light green to dark green without significant increase in viscosity. The product was diluted with chloroform and filtered under vacuum filtration using a 0.22 μm membrane filter. The filtrate was further filtered through an alumina powder. The filtered product was precipitated from cold methanol and the supernatant was decanted and centrifuged. After centrifugation the excess solvent was again decanted and very small amount of product was retrieved. The product, which was found clung on the wall of the centrifugation tube, was flushed by a stream of nitrogen gas to remove the remaining solvent. Eventually, it was dried up overnight using an oven at 65 ^{o}C and kept in a desiccator.

4. Results and discussions

The following sections present the experimental results and their respective discussions. It commences by presenting and discussing the SEM micrograph of the synthesized VACNTs through the thermal CVD method offered in the experimental section. This is followed by the discussion about the surface modification of vertically aligned CNTs using a plasma treatment as well as morphological studies from their SEM images. Later on, an XPS measurement for the plasma treated VACNT samples along with the pristine VACNTs are presented to show the effect of the plasma treatment on the surface functionality of the VACNTs. The preparation of VACNT/PMMA composite *via* ATRP polymerization is also presented using the two routes mentioned in section 3.3.4. Subsequently, the products are validated using Raman, SEM, STEM, FTIR and ^{1}H-NMR measurement. The mechanical properties of the pristine VACNTs and the composite material are also studied using compressive test. Ultimately, some potential application areas regarding the produced VACNT/PMMA composite material are discussed.

4.1. Synthesis of VACNTs

Following the procedure discussed in section 3.3.1., the VACNTs were prepared by Professor R. Silva´s group in University of Aveiro. To grow the aligned CNTs a 1cm by 1 cm silicon substrate containing iron nano-particles as a catalyst supported by alumina were used. Here the iron nanoparticles act as a center (nucleus) for the growth of the vertically aligned CNTs. However, to grow well-aligned and long nanotubes, the size of the iron nanoparticles has to be neither too big nor too small. Below some minimum cut-off value carbon nanotubes cannot grow at all due to the diffusion of the iron catalyst into the silicon substrate during heating. On the other hand, for large size iron nanoparticles, the height of the VACNTs decreases progressively with the increase in the diameter of the iron catalyst. In addition, larger size iron nanoparticles produce larger diameter CNTs with many walls. As a result they require more carbon atoms to build a certain length of carbon nanotubes than required by smaller size iron nanoparticles [88].

A substrate containing iron catalyst already deposited on them, as used in here, leads to a continuous type of VACNTs. In contrast, a substrate without a pre-deposited iron catalyst as in VACNTs from vapor grown CVD method using organo-metallic compounds as the

source of the iron catalyst results in a non-continuous type of VACNTs [89]. In this case, since the iron catalysts are deposited throughout the process from the decomposition of a gaseous organo-metallic compound, mostly ferrocene, long CNTs but with bamboo like structure are obtained. The disadvantage with the former method is that the catalyst used might be coated by amorphous carbon in a process called catalyst poisoning. As a consequence, the CNTs might not grow very long. However, to reduce the effect of catalyst poisoning, using small amount of water vapor was reported to be a solution [43]. The synthesized VACNTs, in our experiment were measured to be in the range of hundreds of micrometer up to a maximum of one millimeter long as observed from their SEM image (figure 10) and their diameter was ~20 nm on average.

In fact, the height and the density of the CNTs produced are dependent on various factors such as the iron catalyst, the alumina support and the flow rates of the gases. The growing parameters and the condition at which the nanotubes are synthesized have also an important control over the vertical alignment of the CNTs. The more the number of CNTs per substrate means the denser and the more rigid the VACNTs get. To assess the quality of the as-produced VACNTs samples, SEM, Raman and XPS analyses have been carried out and the results are presented and discussed in the following sections along with the characterization of these samples after surface modification.

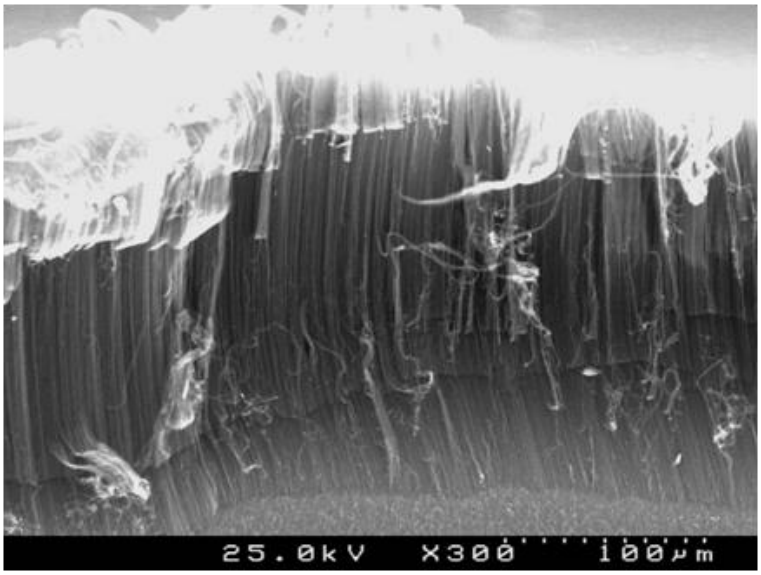

Figure 10: Typical VACNT (~200 μm) used in our experiment produced by thermal CVD.

4.2. Surface modification of VACNTs

Surface modification of CNTs can be carried out using various methods. The most widely used methods have been the wet chemical oxidation methods [47]. However, modifying VACNTs using the wet chemical methods was found to change the morphology of the VACNTs. Hence, other alternative methods have been sought for the surface modification of VACNTs. One of the alternative ways to modify the surface of VACNTs was found to be plasma treatment methods [71-73]. As a matter of fact, a plasma treatment method has already been shown to be successful to modify the surface of nanotubes for grafting poly(glycidyl methacrylate) (PGMA) from non-aligned MWCNTs [90].

Plasma treatment has many advantages over the conventional wet chemical modification methods. First and for most, it modifies VACNTs without damaging their vertical alignment. In addition to this, distinct features such as environmental friendliness, less time consumption and less or no toxic chemical waste have contributed to its outweighed preference [72].

The plasma treatment of VACNTs was carried out using plasma composed of 97:3 ratio of argon to oxygen gas mixture for 10 and 30 minutes at 20 and 2 W, respectively. The influence of the two plasma treatment conditions on the VACNTs were then studied by Raman spectroscopy and the results are presented in figure 14. This part is thoroughly discussed and a detailed comparison to each other to identify which condition has given the better result is presented in section 4.2.2.

The main aim of the oxygen plasma treatment is to create defects on the surface of CNTs by inducing oxygenated functional groups from the surface of the VACNTs. The oxygenated functional groups are attached on the surface the nanotubes from the defects created during the plasma treatment whilst these defects are generated by the reactive oxygen atoms (O•) or ozone (O_3) molecules formed as a result of the dissociation of oxygen molecules (O_2) during an applied potential. These reactive species etch the surface of the VACNTs by reacting with the C-C conjugate bonds to form different kinds of functional groups such as an intermediate molozonides, hydroperoxides, carbonyls, carboxylic acids and hydroxyls.

All those functional groups, except the hydroperoxides, will be produced in higher proportion only if the treatment time is shorter. On the contrary, if longer treatment times are used more hydroperoxides will be produced [73]. Furthermore, the longer treatment time might provide the time for bond reconstruction to take place, which is an unwanted process.

Since the main aim of plasma treatment, here, is to produce more hydroxyl functional group than hydroperoxides the longer treatment time condition at lower power was overlooked and 20 W for 10 minutes treatment condition was chosen to treat the VACNTs for preparing the composite. Two sets of samples, pristine and heat pre-treated were prepared for the plasma treatment at this particular condition. The heat pre-treatment was carried out at 350 ^{o}C for 2 hours in air. The heat pre-treatment was aimed at reducing the amount of amorphous carbon deposited on the VACNTs and to increase the effectiveness of the plasma treatment.

The mechanism through which the plasma treatment occurs was reported by Xu et al. [90]. They have discussed that during plasma treatment, radicals are generated on the surface of the CNTs as a result of the collision between the nanotubes and the ionized atoms (Ar^{+}, O•, O_3), dislodging an electron from the carbon atom that made up the CNTs. Most of the radicals formed on the carbon react with the oxygen molecules or atoms present inside the chamber, to form peroxides and hydroperoxides. Furthermore the ozone molecules would lead to 1, 3-dipolar cyclo-addition (ozonolysis) to the sidewalls of the CNTs following the Criegee mechanism [13].

The reaction of the ozone with the conjugated double bond systems of the CNT sidewall, as in unsaturated hydrocarbons (alkenes and alkynes) can break and inserts oxygen molecules between the double bonds. And hence, the rearrangement of the hydroperoxides and/or the ozonolysis reaction can turn the conjugated double bond system in the nanotubes into hydroxyl (-OH), carboxyl (-COOH) or carbonyl (=CO) functional groups. This mechanism is schematically presented in figure 11.

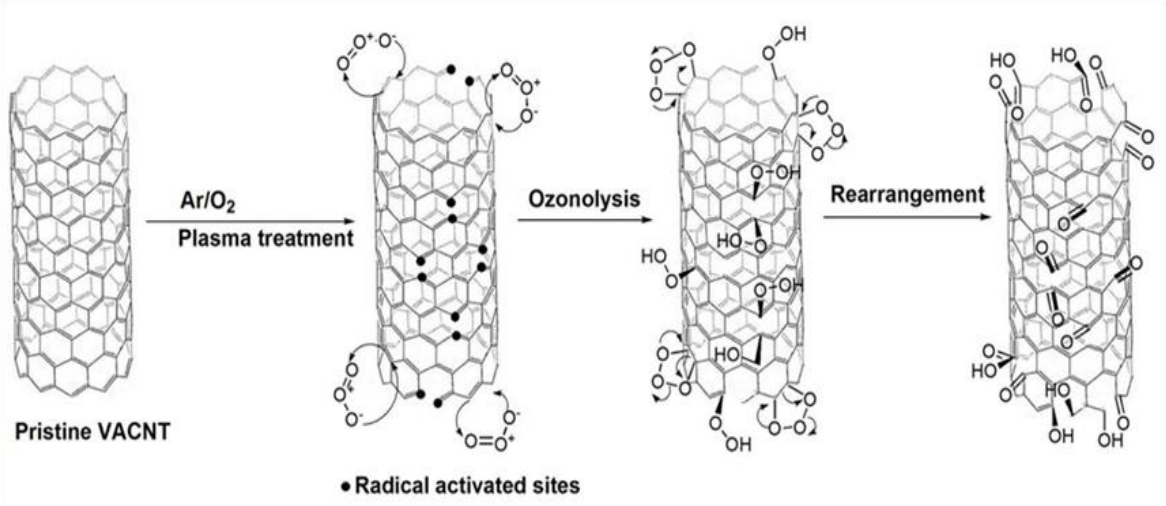

Figure 11: Mechanism for the formation of functional groups on the surface of CNTs through ozonlysis and radical reaction.

4.2.1. X-ray photoelectron spectroscopy (XPS) analysis

XPS is a powerful technique widely used for the analysis of surfaces. It provides information on what types of elements are on the surface as well as how many different elements are bonded to the surface of a material. It has been used to provide chemical bonding information of CNTs in general and vertically aligned CNTs in particular. Several groups have studied the XPS spectra of oxidized SWCNTs and they reported that new C 1s peak around 289 eV attributed to the carboxylic acid groups was observed [65, 91]. Chattopadhyay et al. have carried out XPS analysis to confirm the formation of amide bond (O=C-NH) that link vertically aligned SWCNTs with an amine terminated polyethyleneglycol (PEG) chains [91]. The appearances of N 1s, C 1s, and O 1s at 399.5, 288.4 and 532.5 eV, respectively, have been reported to be the proof for the presence of the amide linkage.

In a similar manner, here the structural and surface characterization was carried out using XPS measurement. The survey scan along with the main peak assignments for the pristine and plasma treated VACNTs are shown in figures 12 (a) and (b), respectively. As expected, the survey scan showed C1s and O 1s core level peaks for carbon and oxygen. In addition, minor peaks in the Fe 2p region have been observed. These signals correspond to the metallic iron catalyst that has been used as the catalyst.

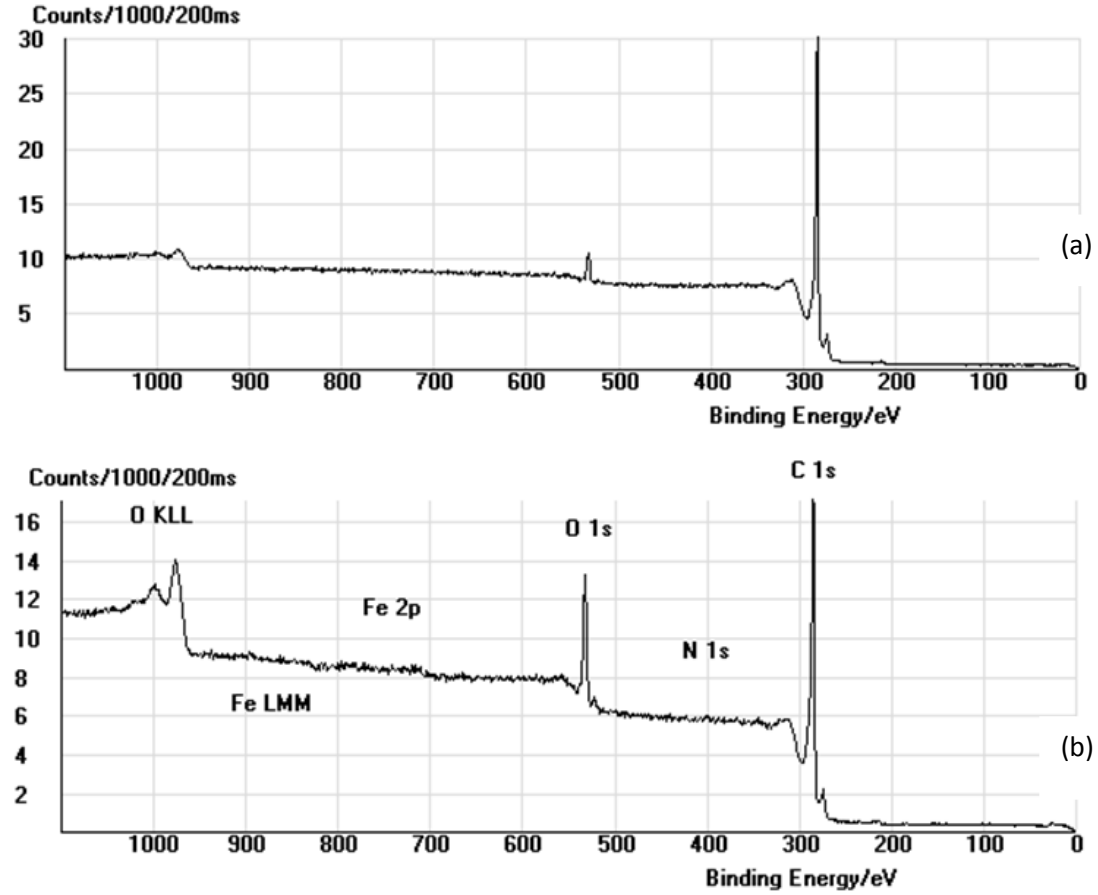

Figure 12: XPS survey scan of (a) pristine and (b) plasma treated VACNTs.

The XPS spectra of the VACNTs before and after the plasma treatment are also presented in figures 13 (a) and (b), respectively. The spectra of the pristine and plasma treated VACNTs showed strong C 1s peaks at a binding energy of approximately 285 eV as well as O 1s signal detected at around 533 eV. The C 1s peak for the pristine VACNTs was found to be more intense than the plasma treated one. On the contrary, the O 1s peak of the plasma treated VACNTs was found to be relatively more intense than the pristine one. The stronger O 1s peak at around 533 eV for the plasma treated sample indicates the increase in the amount of oxygen attached on the surface of the CNT after the plasma treatment, which in turn is an indicator for the formation of defects.

Normally, oxidized CNTs contain a shoulder peak in the range of 286-289 eV whereas pristine MWCNTs have the main signal at 285 eV and a shake-up around 291.5 eV (see figure 13 (a)). The understanding of the C 1s peak of CNTs can also be approached in a different way. The large peak at 284.6 eV with its tail to the higher binding energy

direction can directly be taken as peaks corresponding to the graphene structure. Peaks beyond 290 eV binding energy are considered to be due to the π-π* transition.

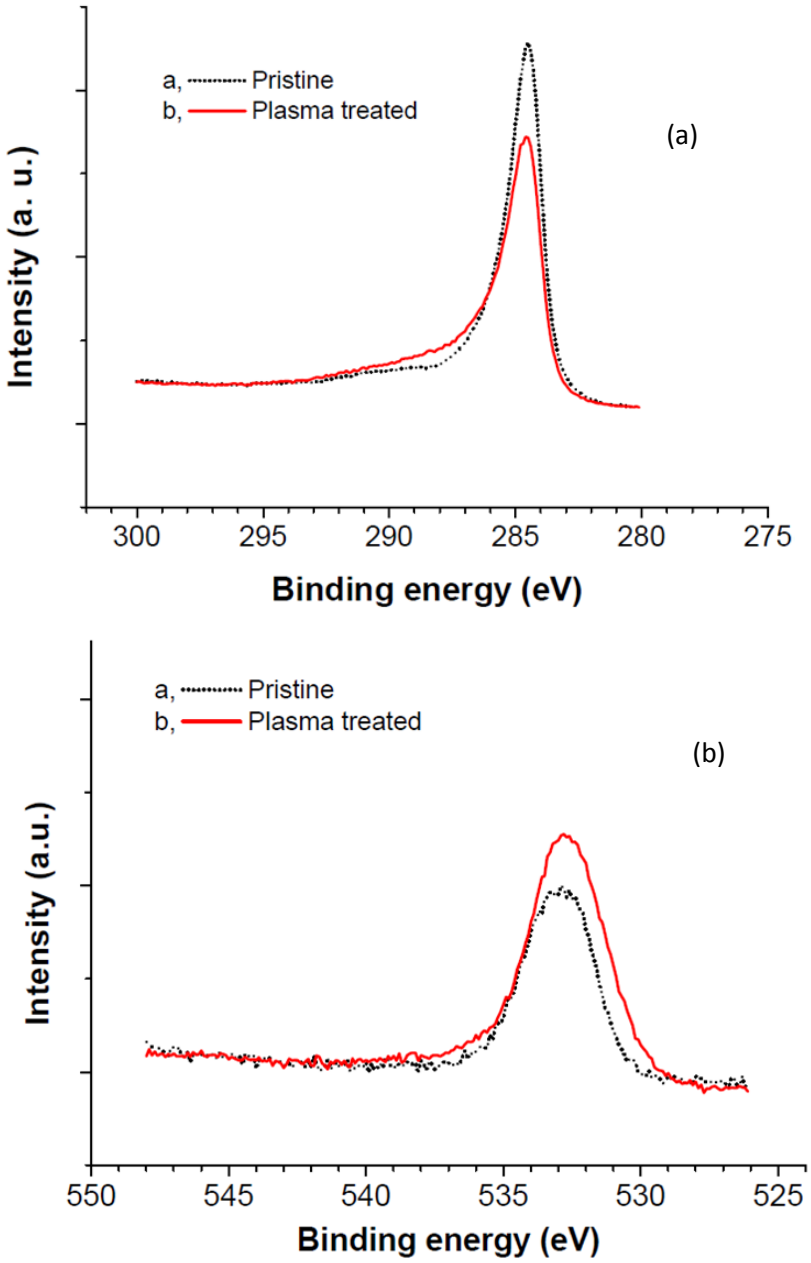

Figure 13: Comparative presentation of (a) C 1s and (b) O 1s XPS spectra of pristine and plasma treated VACNTs, respectively.

The presence of functional groups can also be detected from their corresponding binding energy values at 286.7, 287.9 and 289.2 eV for alcohol/ether (C-O), ketone/aldehyde (C=O) or carboxylic/ester (O-C=O), respectively [65]. From the XPS spectra shown in figure 13, the peaks and the shoulders are smooth and indistinguishable to single out a

specific type of functional group attached in the ranges mentioned. However, the signal for the oxidized VACNT contains a slightly higher shoulder in the range of 286 to 293 eV exhibiting a clear difference as a result of their oxidation from the plasma treatment. In addition there is also a small peak around 287.3 eV. This might be attributed to the carbonyl or hydroxyl groups, which have a signal around 286.7 and 287.9, respectively. Carboxyl groups are not taken into consideration for this particular peak, since its signal is commonly observed at slightly higher binding energy (289.2 eV) than observed here.

The atomic percentage compositions of the two important components that constitute VACNTs are presented in table 2. Qualitatively, the increment in the amount of oxygen from the pristine to the plasma treated VACNTs are also shown in figure 13 (b). From the table the increment in the amount of oxygen is calculated as the difference between the amount of oxygen present before and after the oxidation of the VACNTs and the value indicated ~9 at.% increment. Although the atom percent increment in the amount of oxygen is small, it still indicates oxygen-containing functional groups are grafted on the surface of VACNTs.

Furthermore, a solubility test carried out on scrapped VACNT samples before and after the plasma treatment in ethanol indicated better dispersion of the plasma treated VACNTs sample than the pristine one. This is only possible if the nanotubes are modified with polar groups to interact with the polar solvent molecules. Therefore, it can be said that, the surface modification of VACNTs by oxygen-containing polar functional groups using oxygen plasma was achieved as confirmed from the XPS spectra and solubility test albeit the difficulty in discerning the type of functional groups attached and the low percentage of functionalization.

Table 2: Elemental compositions and oxygen to carbon ratio (in at %) of pristine and plasma treated VACNTs

Sample	Elemental composition (at. %)	
	C (1s)	O (1s)
Pristine	95.67	4.33
Plasma treated	87.32	12.68

4.2.2. Raman spectroscopy analysis

Raman spectroscopy has proved to be an important tool for the non-destructive characterization of carbon nanotubes and carbon based materials. The Raman spectrum of graphite, related allotrope of carbon, has a narrow peak, which is labeled as "G-band" around 1580 cm^{-1}, and diamond another allotrope of carbon has a single peak at 1332 cm^{-1}. CNTs, on the other hand, have three major characteristic absorption peaks. These characteristics peaks are radial breath mode (RBM), D-band and G-band, which are observed around 200 cm^{-1}, 1350 cm^{-1} and 1580 to 1600 cm^{-1}, respectively.

RBM occurs due to the displacement of the carbon atoms along the radial direction and its frequency (ω_{RBM}) varies inversely with the diameter of the nanotubes. This is convenient for the determination of the diameter of SWCNTs. Small diameter SWCNTs have RBM peaks below 200 cm^{-1}. However, larger diameter SWCNTs or MWCNTs usually lead to a weak and broadened signals [92].

The G-band is an intrinsic feature of CNTs closely related to the vibrations of the graphitic sp^2 structure. In this mode the carbon atoms are displaced tangentially. The G-band can have two components G^+ around 1590 cm^{-1} and G^- around 1570 cm^{-1}. As in RBM, the lower frequency component (G^-) is essentially dependant on the diameter of the nanotubes. Thus, it helps in the designation of chirality in SWCNTs as well [93]. However, MWCNTs have only one G-band as an asymmetric characteristic line shape close to the graphite frequency, since the splitting of G^+-G^- bands are generally unobservable as in SWCNTs.

The D-band (disorder band) is observed due to the presence of impurities and defects in the nanotubes. These bands are special in such a way that they change their frequency when the laser excitation energy changes as a result of second-order scattering process and a Raman intensity enhancement [94]. D-bands along with G-bands are helpful in determining the relative amount of surface modification achieved during any surface modification processes by taking the ratios of their intensities or areas.

In addition, Raman spectroscopy can also be used to provide evidence whether polymers are grafted on the surface of CNTs by physical adsorption or covalent bonding. Nan et al. have demonstrated the use of Raman scattering for the identification of covalently grafted and physically adsorbed polymer matrices [95]. Primarily, they have prepared vertically

aligned SWCNTs modified through surface condensation *via* amide bond formation and through physical adsorption. And then Raman measurement was taken before and after both modified-SWCNT samples were exposed to sonication in ethanol for a certain time. The Raman spectra for the covalently modified SWCNTs were reported to be very similar before and after the sonication whereas very different Raman spectra were observed for the modified SWCNTs via physical adsorption.

The orientations of VACNTs on the substrate have also been demonstrated using a Raman scattering technique, known as polarized Raman spectroscopy. Papadimitrakopoulos et al. have reported that the G-band of the polarized Raman spectra of vertically aligned SWCNT samples recorded maximum intensity when the polarization of the incident light was parallel to the nanotube axis. In contrary, the G-band intensity went down to the minimum when the polarization of the incident light was perpendicular [96].

To study the effect of different energy plasmas and different treatment times on the surface modification of VACNTs, Raman measurement was taken from samples treated at 20 W for 10 minutes and 2 W for 30 minutes. And the Raman spectra of both plasma treatment conditions used are plotted and the spectra are shown in figure 14. From the figure both plasma treated samples at 20 W and 2 W have showed a lower intensity G-bands than the pristine one. On the contrary, their D-bands are almost similar. The lower intensity G-bands for the plasma treated samples were expected since the plasma treatment was supposed to create defects by attaching oxygen-containing functional groups on the VACNTs by breaking some graphitic bonds that contribute to the G-band. However, instead of similar D-bands, an increase in the D-bands was expected, contemplating an increase in the defects as a result of the plasma treatment. Perhaps, the similarity in the D-bands after the plasma treatment can be attributed to two counterbalancing effects occurred during the plasma treatment process namely, defect formation and amorphous carbon oxidation.

As compared to each other, both treatment conditions gave more or less similar results and the observed differences are minor. Nonetheless, a slightly narrow and shorter G-band spectrum with D-band to G-band area ratio (A_D/A_G) of 0.62 was observed for the sample treated at 20 W as shown in table 3. This indicates better influence of the plasma on the nanotube forests. This can be explained based on the spectra shown in figure 14. The

Raman spectrum of the sample treated at 20 W for 10 minutes showed slightly less intense and narrower G-band spectra at full width half maximum (FWHM) revealing the more damage incurred on the graphitic structure as a result the higher plasma power. This damage created more defects in the form of oxygenated functional groups. Since the oxygen plasma treatment is used to attach more oxygenated functional groups, the Raman result favors the treatment condition at 20 W for only 10 minutes as slightly better method than 2 W for 30 minutes condition. This is in agreement with a previous study carried out using an oxygen plasma at a specific power and varying time conditions that has revealed shorter treatment time as a better and effective way than longer treatment time [73].

Table 3: The area ratios of the D-band to the G-band of the pristine, 2 W for 30 minutes and 20 W for 10 minutes oxygen plasma treated VACNTs.

Samples	Plasma treated		Pristine
	20 W for 10 minutes	2 W for 30 minutes	
A_D/A_G ratio	0.62	0.53	0.46

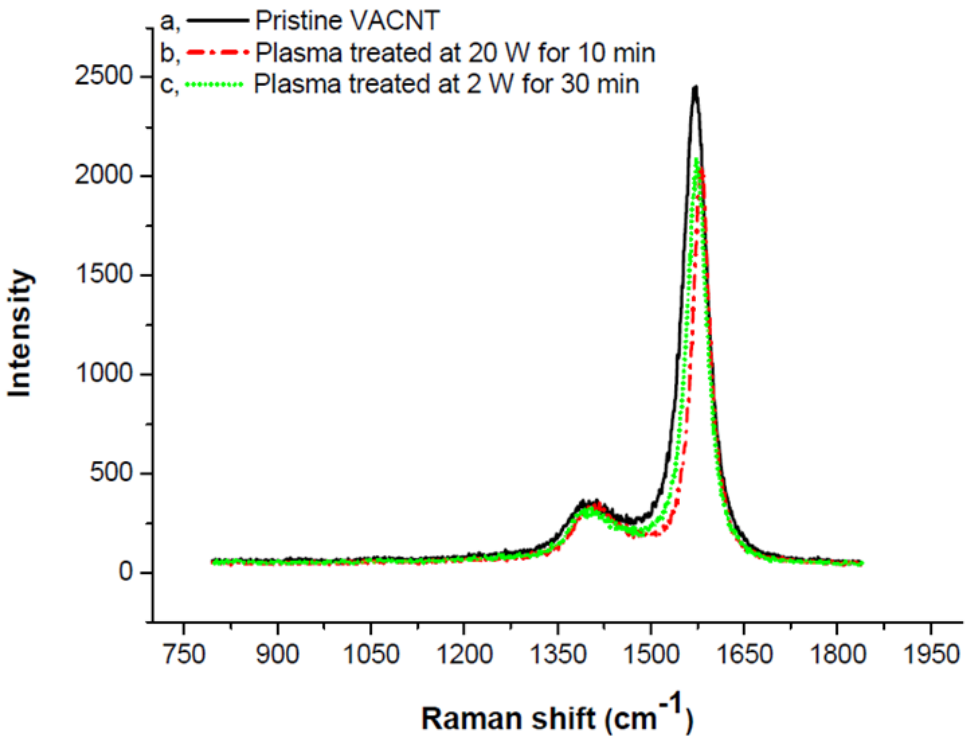

Figure 14: Raman spectra of the pristine VACNT (a) and plasma treated VACNTs (b and c) at 20 W for 10 minutes and 2 W for 30 minutes, respectively.

In addition to realize the effect of the plasma treatment on the quality of VACNTs and to study the presence of surface modification, Raman spectra were collected for each sample. The Raman spectra of the pristine, heat+plasma treated, and plasma treated VACNT samples are presented in figure 15. Like any other CNTs, their spectra contain the characteristic D- and G-bands. The G-bands are observed around 1580 cm^{-1}. Whereas, the D-bands associated with disorder are observed around 1400 cm^{-1}. The D-band is slightly higher than the normal value. This might be associated with second-order scattering effect and Raman intensity enhancement phenomena, which are dependent on the laser excitation energy [94].

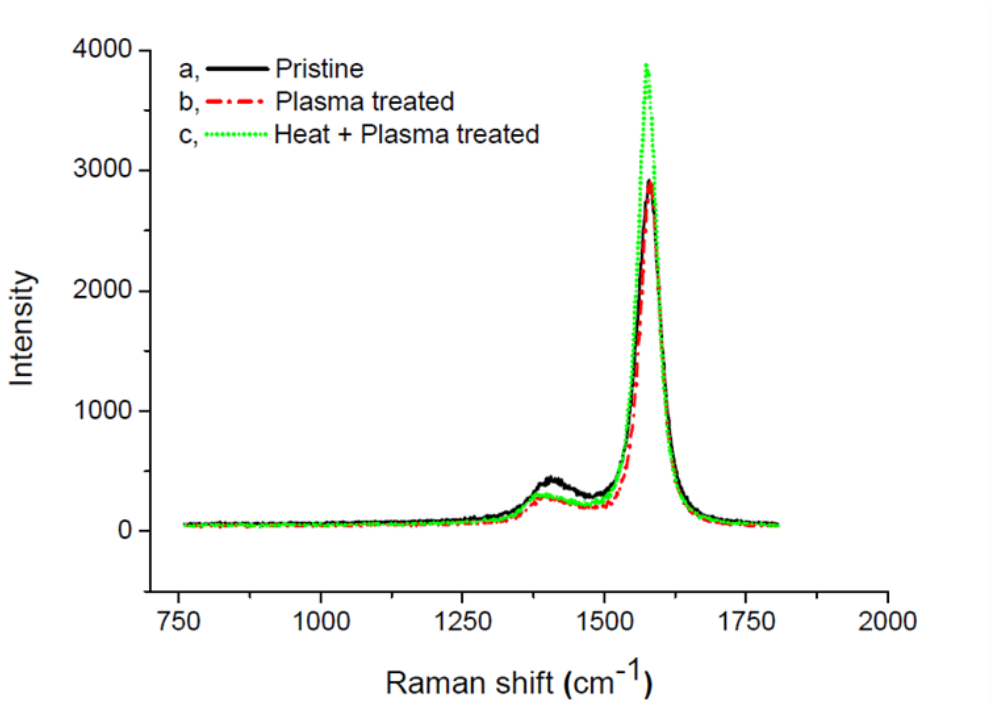

Figure 15: The Raman spectra of pristine (a), plasma treated (b) and heat+plasma treated (c) VACNT samples.

The ratios of the intensities of the D-band to that of the G-band are commonly used in identifying the purity, i.e. presence of defects. Likewise, similar intensity D- and G-bands are indicators of higher amount of structural defects [97]. Hence, the higher intensities of G-bands observed in both pristine and plasma treated samples in this study are indicators of the high quality of our thermal CVD-grown CNT forests. Especially, the G-band observed for heat+plasma treated sample has the most intense G-band and is an indicator of its highest quality. Indeed, this was obtained since the heat pre-treatment before the

plasma modification had reduced the amount of the amorphous carbon deposited by oxidizing them. In addition, some of the kinked or broken bonds of the graphitic structures on the VACNTs can be reformed as a result of the thermal treatment. The thermal pre-treatment anneal the CNTs as in the thermal annealing process that is used for the purification of CNTs [93]. On the other hand, the pristine VACNT signal contains lower G-band and slightly higher and broader D-band. Again, the broad D-band is associated with the purity level of CNTs. The broader the D-band is the, the less pure the CNTs are and vice versa [97].

The intensity ratios of the D-band to G-band for each VACNTs samples were calculated and tabulated in table 4. As expected, the heat+plasma treated sample showed the lowest I_D/I_G ratio in comparison to the other samples. Similarly, the plasma treated sample has also showed lower D-band to G-band intensity ratio than the pristine sample albeit the difference is still minor than between the pre-heat treated and pristine samples. The relatively bigger difference between pristine and heat+plasma treated sample arises again from the removal of the amorphous part that contributes to the D-band in the pristine sample.

Table 4:The intensity ratios of D-band to G-band of the pristine, heat+plasma treated and plasma treated VACNTs.

Samples	Heat+plasma treated	Plasma treated	Pristine
I_D/I_G ratio	0.08	0.11	0.16

It is also evident from figure 15 that the D-band intensities of the pristine and plasma treated samples are different with the pristine having the highest. As a result the pristine have the highest I_D to I_G ratio (table 4). Although identical D-bands are observed for the plasma treated and heat+plasma treated samples, yet their G-bands are quite different. Therefore, it can be summarized that the heat+plasma treated sample is of high quality and more graphitic than the others, followed by the plasma treated sample.

4.2.3. Morphological studies

The morphological study of CNTs and in fact of any microscopic material for that matter can be carried out using scanning electron microscope (SEM) and scanning transmission electron microscope (STEM). SEM is one type of electron microscopy technique that images the surface of a sample by scanning it with high-energy beam electrons. It provides a general idea about the morphology and purity of CNTs as well as their presence, alignment and distribution on a substrate as well as in a composite material. It has also a simple and straightforward sample preparation. Even though imaging individual CNTs is challenging, it can magnify them up to a maximum resolution of 1 nm [11].

A more detailed image CNTs is obtained from scanning transmission electron microscope (STEM). STEM is a type of transmission electron microscope (TEM) that images a sample by collecting transmitted electrons through a sufficiently thin specimen (<200 nm) using a detector. The image contrast is obtained when the collimated electron beams are intercepted by atoms in the sample. However, unlike other conventional transmission electron microscopy techniques, the electron beams are focused into a narrow spot and scanned over the sample in a raster. One disadvantage of STEM is that under typical illumination conditions, CNT samples are prone to degradation. This limits the time during which CNT samples could be analyzed. Often, both SEM and STEM techniques show the best data than representative data depending on the skill, experience and patience of the operator [11].

The morphological images of the pristine, heat+plasma and plasma treated VACNTs samples are studied using their SEM images. Their images are shown in figure 16. Literally, VACNTs are made up of vertically arranged CNTs supporting each other like a dense forest. The SEM image of the pristine VACNTs appears containing an amorphous carbon deposited over its surface (figure 16 (a)). This is in agreement with the highest I_D/I_G ratio calculated as compared to the other samples analyzed by the Raman spectroscopy. After the plasma treatment the amorphous carbons are partially oxidized and removed from the surface of the nanotubes leaving a jagged surface in contrary to a more or less even and leveled surface observed at the beginning before the plasma treatment as shown in figure 16 (b). Moreover, most part of the heat pre-treated sample is found to be free from the amorphous carbon, which is also in agreement with the Raman analysis, i.e. the lowest

I_D/I_G ratio. However, the heat pre-treatment has also oxidized the iron nano-particles, which anchors the nanotube forests grown on the substrate. As a result, these forests became vulnerable to erosion and were washed away from the substrate while they were further processed in the subsequent solution processing methods.

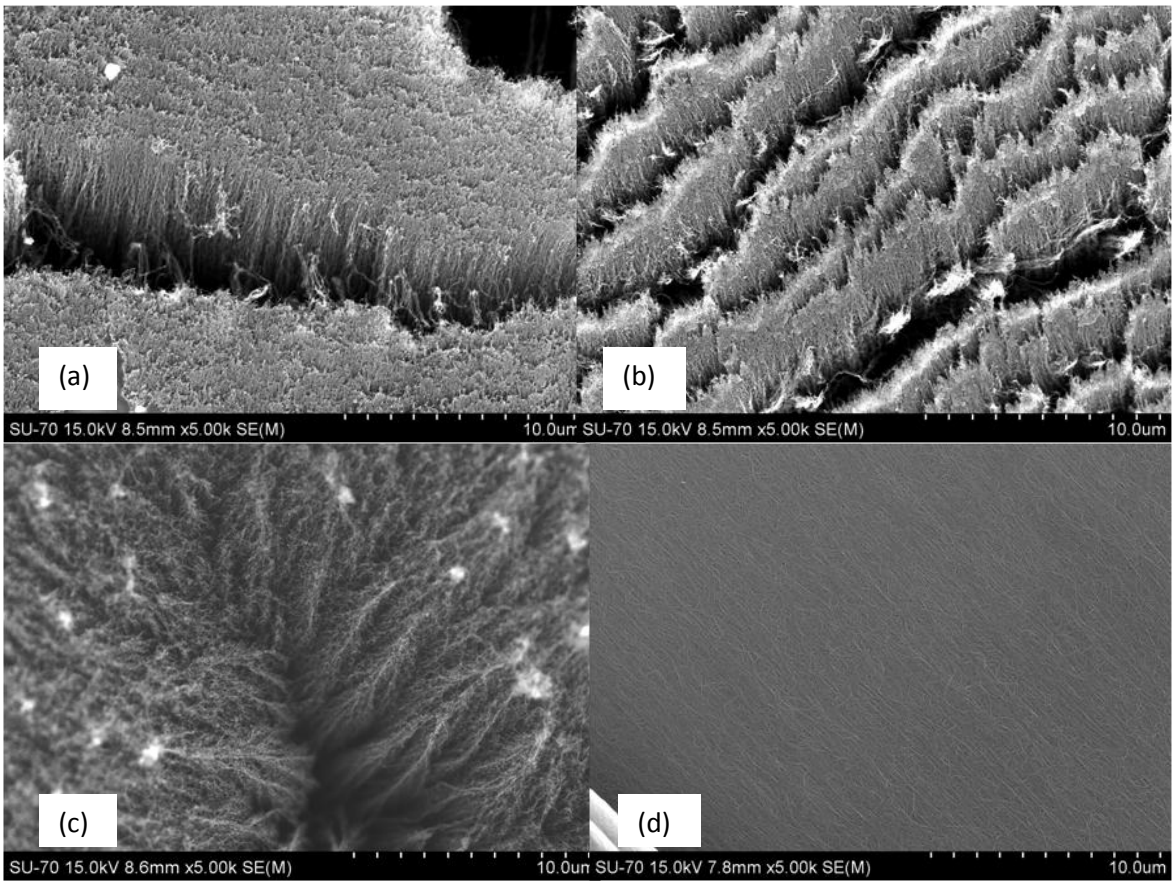

Figure 16: SEM images of (a) pristine, (b) plasma treated, (c) heat+plasma treated, and (d) nitric acid treated VACNTs.

For comparison, the effect of chemical modification of VACNTs using the wet chemical oxidation methods, particularly using nitric acid has also been carried out and the morphology was compared with the plasma treated samples. And, the SEM result for the nitric acid treated sample has revealed that the vertically aligned CNTs are collapsed as shown in figure 16 (d). Thus, in our experiment the surface modification of VACNTs using nitric acid was regarded as the least viable method of choice, which is in contrast to the report by Sun et al. [84].

4.3. ATRP polymerization of MMA from VACNT surface

As discussed in section 2.5., CNTs can be modified by polymers either covalently or non-covalently depending on the nature of their interaction. The covalent modification itself can further be carried out using two different strategies: *"grafting to"* and *"grafting from"*. The *"grafting to"* approach involves the synthesis of pre-formed polymers with a specific molecular weight containing reactive groups or radical precursors. In the subsequent reaction the polymer chains are attached to the surface of the CNTs through addition reactions. A disadvantage of this method is that the grafted polymer density is limited because of the relatively low reactivity and high steric hindrance of the macromolecules.

On the other hand, the *"grafting from"* approach consists in a surface-initiated polymerization strategy, which involves the growing of polymer chains from the CNTs surface *via in situ* polymerization of monomers initiated by chemical species immobilized on the CNT sidewalls and edges. Due to the high reactivity of the monomers, this method is highly efficient. In addition it allows the design, control and tailoring of the grafted polymer. The *"grafting from"* approach has been demonstrated using the well established living radical polymerization techniques such as atom transfer radical polymerization (ATRP) [80, 81].

ATRP, as mentioned in section 2.6., is a type of living/controlled radical polymerization technique, which can be used for the grafting of polymers on the surface of CNTs from the already attached surface-derived initiators. The main components in the ATRP polymerization process include a transition metal species (Mt^n), generally copper is used, which can form a transition metal complex (Mt^n/L) with a complexing ligand (L) by increasing its oxidation number, as well as an alkyl halide initiator (P_n-X) containing CNT that generates higher oxidation state metal halide complex (X-Mt^{n+1}/L) to form an organic radical (P_n*) [81, 98]. Ultimately, the generated radicals on the initiator grafted CNT (P_n*) combine with monomers to grow a polymer chain from the surface of the nanotubes. The mechanistic illustration is presented in figure 17.

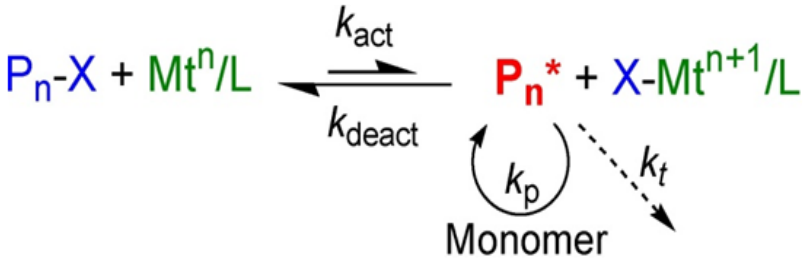

Figure 17: The mechanism of ATRP reaction. Note: P_n-X represents initiator grafted CNT [98].

In our work the grafting of methyl methacrylate (MMA) from initiator modified VACNT has been demonstrated using this ATRP polymerization technique. In fact, various authors have already demonstrated the grafting of different kinds of polymers in general and PMMA in particular on the surface of CNTs and vertically aligned CNT samples for various reasons such as to prepare superhydrophobic surfaces, temperature responsive surfaces and so on [55, 82-85]. However, here the aim of grafting PMMA from VACNTs is to impart more mechanical stability to the aligned CNT structure. PMMA was chosen as the polymer matrix for it is a well studied material and its favorable combination of chemical and physical properties for easy processing. In addition, its outstanding chemical and physical properties have already represented a suitable polymer component for embedding microscopic and nanoscopic fillers and structures for the preparation of different kinds of hybrid materials [99].

To carry out the grafting of PMMA chains from VACNTs, the plasma treated VACNTs, particularly treated at 20 W for 10 minutes were used. These samples were specifically chosen due to the better plasma modification achieved at this condition as discussed in section 4.2. Actually, the heat+plasma treated samples were found to be much better than the plasma treated samples. However, due to their instability in solution, they were not further used in our study.

To ready the plasma treated VACNT samples for the ATRP polymerization process, the hydroxyl groups, one of the functional groups attached during the plasma treatment will be directly modified with a bromine-initiator. In fact, the effectiveness and the success of the ATRP polymerization depends on the percentage of hydroxyl groups produced and modified by the initiator. In a previous study, the amount of hydroxyl groups formed by the plasma treatment has also been reported to be higher when the treatment is carried out

at higher power for shorter treatment time, as was followed in this work [71]. Therefore, it is expected that sufficient amount of hydroxyls groups are attached after the plasma treatment. However, the unavailability of the XPS instrument nearby hampered the precise and rigorous study on the quantity of hydroxyl groups attached.

Anyhow, the attached hydroxyl groups produced by the plasma treatment were reacted with 2-bromo-2-methylpropionylbromide, an ATRP initiator that immobilizes bromine-containing molecules on the surface of the VACNTs following the two procedures given in section 3.3.4., i.e.:

a. GO-modified pathway [86] and
b. CNF-modified pathway [87].

Then, the initiators were used as a precursor for the subsequent ATRP polymerization reaction of MMA using the corresponding pathways. The general reaction is depicted schematically in figure 18. Comparatively, the products from the two methods (GO-modified and CNF-modified) were studied using SEM, STEM, FTIR and Raman spectroscopies to determine which pathway led to a better result.

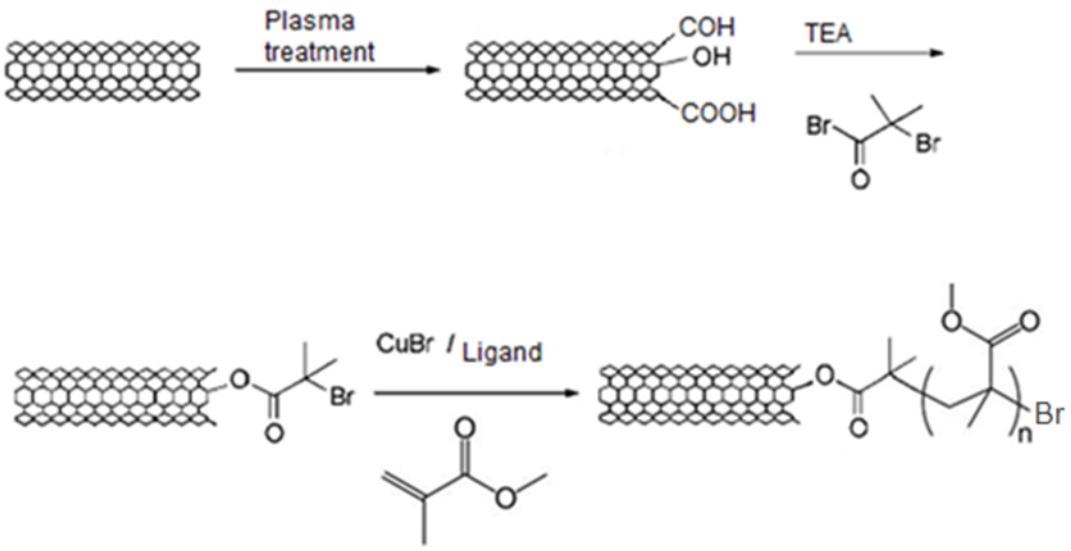

Figure 18: Reaction scheme of the ATRP polymerization of MMA from bromine-initiator-containing VACNT.

4.3.1. Morphological studies

As in section 4.2.3., here also the morphological and structural studies were carried out using the images obtained from SEM and STEM. The results at high magnification clearly showed the presence of a polymer matrix in the composite produced through both *in situ* polymerization methods surrounding the CNTs as depicted in figures 19 (b) and (d). At low magnification however, the composite produced by both methods looked like a porous material as a result of solvent-induced flattening of some parts of the aligned CNT structure. The cause for this behavior is attributed to the polymerization reaction of CNTs in a liquid media. In fact the challenging task while working with VACNTs is producing composites preserving the CNTs´ vertical alignment. However, the liquid system employed in the ATRP initiator attachment and ATRP polymerization stages make it almost impossible.

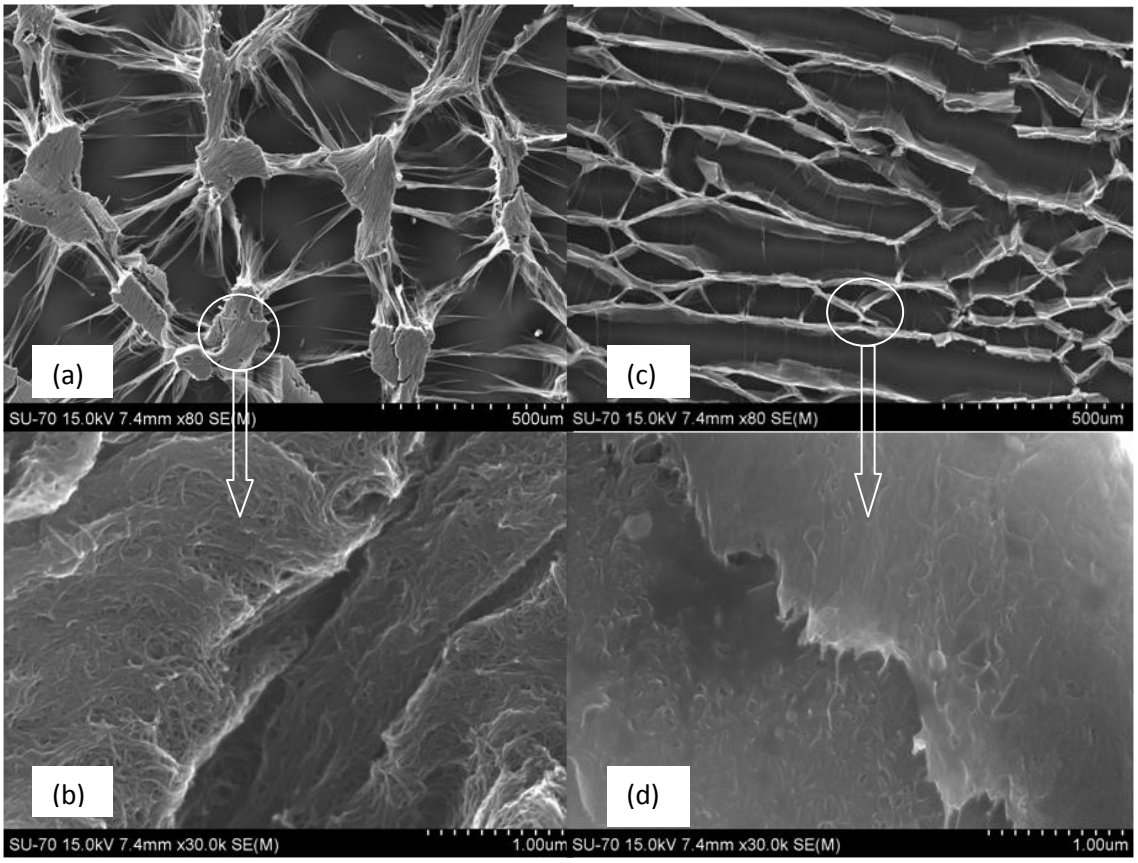

Figure 19: VACNTs/PMMA composites prepared using GO-modified (a, b) and CNF-modified (c, d), ATRP methods. The VACNTs were modified using an Ar/O_2 plasma at 20W for 10 minutes.

Nonetheless, comparison of the SEM images (figures 19(a) and (c)) of the composites prepared by the two methods revealed a better morphology of the composite processed by the GO-modified method. The GO-modified method preserved the vertical alignment of the CNTs better than the CNF-modified whereas the composite prepared by the CNF-modified method comprises a more stacked VACNT structure, which appears as long, stretched walls and at some parts having honeycomb-like structure (figure 19 (c)).

Perhaps the difference in the morphology of the two methods might be dependent on the time spent for the two reactions to be completed. In the GO-modified method the VACNT samples were processed for a total duration of 42 hours whereas in the CNF-modified method they were processed for 72 hours in a liquid media. Therefore, to prepare a composite by GO-modified method required 30 hours less than the CNF-modified method. As a result, wider areas of the VACNTs´ structure and morphology are preserved than in the CNF-modified method.

On the other hand, since the CNF-modified method had allowed the VACNT samples to react for longer time, its composite is covered more with the polymer than the GO-modified method. This can be observed from the SEM images of the composites at higher resolution presented in figures 19(b) and (d)). The observed result might be the reflection of two important factors. The first factor is the time spent for the reaction to be completed in the initiator and polymer grafting stages. CNF-modified method has taken longer time (total of 30 hours more) during the initiator and polymer grafting stages. This might allow more initiators to be attached on the VACNT and consequently more MMA monomers will be reacted to grow PMMA chains.

The second factor is the variation in the chemical reagents used to carry out each processing methods. In the GO-modified method the metal catalyst was used in the bulk form using copper wire whereas in the CNF-modified method the catalyst was in the form of a readily soluble copper salt (Cu(I)Br) powder. Therefore, CNF-modified method is expected to be more efficient than the Go-modified method as a result of better solubility of the catalyst. In fact, it has been reported that the yield of in ATRP polymerization reaction to be dependent on factors such as the amount of initiator grafted, the reaction time and solubility of the copper catalyst used [81, 83].

Furthermore, in both composite materials, the neighboring CNTs are leant on each other and packed together to gain more rigidity and strength. However, the composite from CNF-modified method showed a more packed structure. This packing structure is observed as a result of the "zipping effect" that draws the nanotubes together to form a stacked structure caused by the surface tension of the solvent and the van der Waals forces between the carbon nanotubes [43]. As a consequence, the composite materials prepared are more rigid than the pristine VACNTs. This property will be discussed further more systematically in section 4.4.

Note: Despite some similarity in the products obtained by both methods in terms of liquid-induced collapsed morphology, the critical differences observed in the processing conditions and morphology favored the CNF-modified method as more feasible than its counterpart due to the previous discussions. Therefore, the following characterizations will focus solely on the composite prepared by the CNF-modified method albeit the proton nuclear magnetic resonance spectra (^{1}H-NMR) of both samples are shown in figure 22 to highlight how inefficient the GO-modified method was.

In addition to the above discussion, the presence of the polymer was also confirmed by STEM. Both the TEM and the SEM image at 100 nm showed the presence of a polymer surrounding the CNTs. Especially the TEM image have showed a distinct polymer layer surrounding the CNT with a thickness of ~10 nm as indicated by the arrow in figure 20 (a). In addition to this, the STEM images could provide information about how the polymer chains are attached with the CNTs i.e. whether they are physically adsorbed or covalently bonded. Thus, the specimens for the STEM analysis were prepared by sonicating a composite in ethanol for 30 minutes and by immersing standard TEM copper grids into the suspension and taking out to dry. This process would ensure the removal of any ungrafted or physically adsorbed polymer chains, and any sign of polymers observed in the STEM image should be due to covalently bonded polymers to the CNTs. Therefore, one can claim that the PMMA chains are grafted covalently on the VACNT through covalent bonding rather than mere physical adsorption.

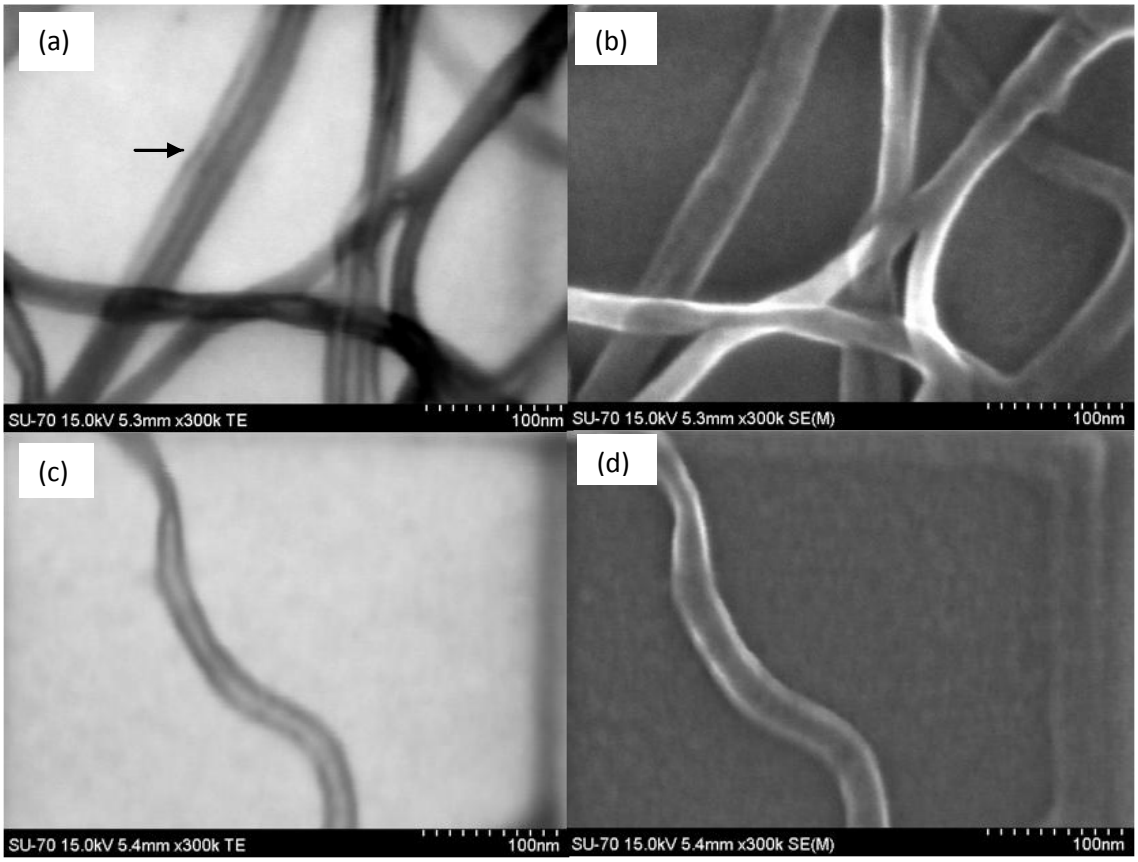

Figure 20: STEM image of pristine VACNT and VACNT/PMMA composite via CNF-modified method: (a) and (c) TEM and (b) and (d) SEM images.

As discussed in section 2.6., surface-initiated *in situ* ATRP polymerization of vertically aligned CNTs have been studied by numerous authors who have followed different strategies in modifying the surface of the aligned CNTs by an initiator molecule for the subsequent polymer grafting process [57, 84 and 85]. Interestingly, in all the three papers referred wet chemical functionalization of the VACNTs has been followed despite the fact that processing in liquid media has been reported to cause solvent-induced collapse and zippering of VACNTs due to capillary and van der Waals forces [7, 43]. Sun et al. have used nitric acid oxidation of VACNTs for two hours and then they immobilized amine group containing molecule, aminopropyltrimethoxysilane (ATMS), to the nitric acid treated aligned nanotubes. This was followed by reacting with ATRP initiator for 6 hours [84]. Subsequently, the polymerization of *N*-isopropylacrylamide (NIPAAm) was carried out in water/methanol solution using ATRP condition for 100 minutes.

On the other hand, Pastine et al. [57] and Matrab et al. [85] have initially grafted ATRP initiators containing diazonium salt, and azides from the surface of VACNTs using electrochemical reduction and nitrene insertion methods, respectively without the need of any acid or plasma pre-treatment. Afterwards, Pastine et al. reported the ATRP polymerization of *N*-isopropylacrylamide (NIPAAm) from VACNTs in a flask containing water/methanol solutions and the grafted substrate was later washed with copious amounts of water and acetone. Whereas, Matrab et al. reported the grafting of polymethyl methacrylate (PMMA) from the surface of aligned CNTs at 90 ºC for 6 h.

However, the preserved vertically aligned CNT structures from these methods were surprising; particularly that of Sun et al [84]. In our work the chemical modification of VACNTs carried out using nitric acid leads to a totally collapsed structure as shown in figure 16(d). In fact their results are also quite in sharp contrast from those obtained in the present study as well as by others, namely Matrab et al. [85]. Besides, Sun et al. had also reported that keeping the aligned CNTs in high vacuum environment, such as in the chamber of SEM improve the strength of the nanotubes during solution processing. However, no significant improvement has been observed in our work even after keeping the nanotubes for more than two days in the high vacuum chamber of the plasma CVD apparatus that could surmount the solvent-induced collapse. Yet, similar to this work with the heat+plasma treated VACNTs samples, Matrab et al. have reported the detachment of the aligned CNTs from the silicon substrate [85].

The growing conditions of the forests from the three authors mentioned have also been compared to ours to observe any dissimilarity that contributes to the different outcomes obtained in our method. And of course, Sun et al. and Matrab et al., have followed a method that could result in non-continuous types of nanotubes as elaborated in section 4.1.

Briefly, Sun et al. [84] have prepared the nanotubes from the pyrolysis of iron phthalocyanines (FePc) containing both the metal catalyst and carbon source required for the growth of the nanotube. The pyrolysis of FePc was performed under an Ar/H_2 (1:2 v:v) flow of 50–60 sccm at 600–900 ^oC on a 1×1 cm^2 cleaned silicon template in a flow reactor consisting of a quartz glass tube for 1 hour. The diameters of the nanotubes were between 15-50 nm (ca. 39.7 nm on average). Likewise, Matrab et al. [85] have grown the nanotube forests on *n*-doped silicon substrate by aerosol-assisted catalytic chemical vapor deposition

using a starting solution composed of ferrocene (5 wt.%) dissolved in toluene. Then the aerosol was carried by an argon flow and pyrolysed at 850 ˚C during 7 min. The lengths of the nanotubes were 130 μm with external diameters ranging between 10 and 100 nm. Evidently, both methods are completely different than our preparation method.

On the other hand, Pastine et al [57] argued that the structural integrity of the nanotube forests on the surface of the substrate is limited by their weak adhesion. Thus to address the issue regarding the weak adhesion and the propensity of the nanotubes forests to deformation due to the strong van der Waals between them and the strong capillary forces observed when exposed to solvent, they have used bigger diameter (10 nm thick) iron catalyst film and a high ethylene concentration (pure ethylene at 200 sccm for 10 min) at 750 °C. They produced CNT forests with a diameter of approximately 40 nm. According to the authors the vertical alignment of the nanotubes is preserved due to an increased forest adhesion to the substrate achieved by their improved VACNTs synthesis conditions and the observed durability was attributed to a cementing effect caused by amorphous carbon deposited on the nanotube surface during growth.

As a matter of fact, we have also observed similar amorphous carbon deposition on our CVD synthesized samples (figure 16(a)). However, the employed plasma treatment method in our method for the surface modification of the nanotubes have removed significant amount of the amorphous carbons (Figure 14, 15 and 16(b)). Therefore, their importance as a cementing agent is less significant in contrast to the report by Pasine et al. Besides, in our experiment the synthesis condition followed for the synthesis of the nanotube forests involve only -2 nm iron catalysts and 10 sccm ethylene gas flow as compared to 10 nm iron catalyst and 200 sccm ethylene gas flow used by Pastine et al. Hence, the smaller diameter and the lower ethylene concentration condition used in our synthesis might also be accountable for the collapsed structure obtained, despite the fact that still our nanotube forests were not eroded as in Matrab et al. [85].

Xu et al. have used nitrogen plasma, created by corona discharge at normal atmospheric pressure to modify non-aligned MWCNTs, which is comparative to our work in using plasma treatment for surface modification [90]. Then they transferred the treated nanotubes into glycidyl methacrylate (GMA) to perform surface-initiated graft polymerization for 4 hours at 70 ºC under ultrasonication to yield a composite with a grafting ratio of about 22

wt%. In view of the reduced number of steps involved this approach might be considered as an alternative route to be explored. Nonetheless, this polymerization technique did not allow control over the length of the polymer chains nor the composition, as other living polymerizations, for example ATRP do. Moreover, the 4 hours long ultrasonication at 70 ^{o}C used for the polymerization of GMA was also considered to be a major risk for our work.

And very recently, during the course of this study, the functionalization of aligned MWCNTs with similar epoxy polymer (PGMA) through a one-step initiated CVD (iCVD) has been successfully demonstrated by Ye et al. [100]. In this method no solvent has been involved any stage of the process at all as a result the forest structure was reported to be completely preserved.

4.3.2. Fourier transform infrared spectroscopy (FTIR) analysis

The electron microscopy methods have highlighted the presence of the polymer matrix surrounding the VACNTs and more information regarding the immobilized chemical functional groups onto the aligned nanotubes after the plasma treatment and ATRP polymerization was offered by FTIR analysis. The FTIR studies carried out on the plasma treated, heat+plasma treated, VACNT composite and commercial PMMA are presented in figure 21. The FTIR spectra are expected to show the presence of the characteristic functionalities of VACNT samples after of the plasma treatment and the functional groups of the polymer grafted on the VACNT. In fact, the preliminary study from the solubility test carried out on the polymer grafted VACNTs sonicated in ethanol showed better dispersion and this suspension was stable for long time.

The FTIR spectra in figure 21 unveiled the characteristic peaks for the carbonyl groups (C=O) around 1730 cm^{-1} for all the samples analyzed. This was expected. For the plasma treated samples the carbonyl signals arise as a result of the carbonyl groups formed during the surface oxidation the nanotubes using the Ar/O_2 plasma. However, the presence of the hydroxyl groups (very broad signal between 3100-3600 cm^{-1}), which were very important to this experiment could not be clearly identified due to the presence of external interference such as moisture with its signal around 3400 cm^{-1}. Even using sodium chloride window, couldn´t solve this problem. The carbonyl signal of the VACNT/PMMA composite material was also observed and here the signals might be due to presence of

plasma induced carbonyl groups, which are unused in the grafting process and/or due to the presence of PMMA polymer matrix that contain (C=O) functional groups.

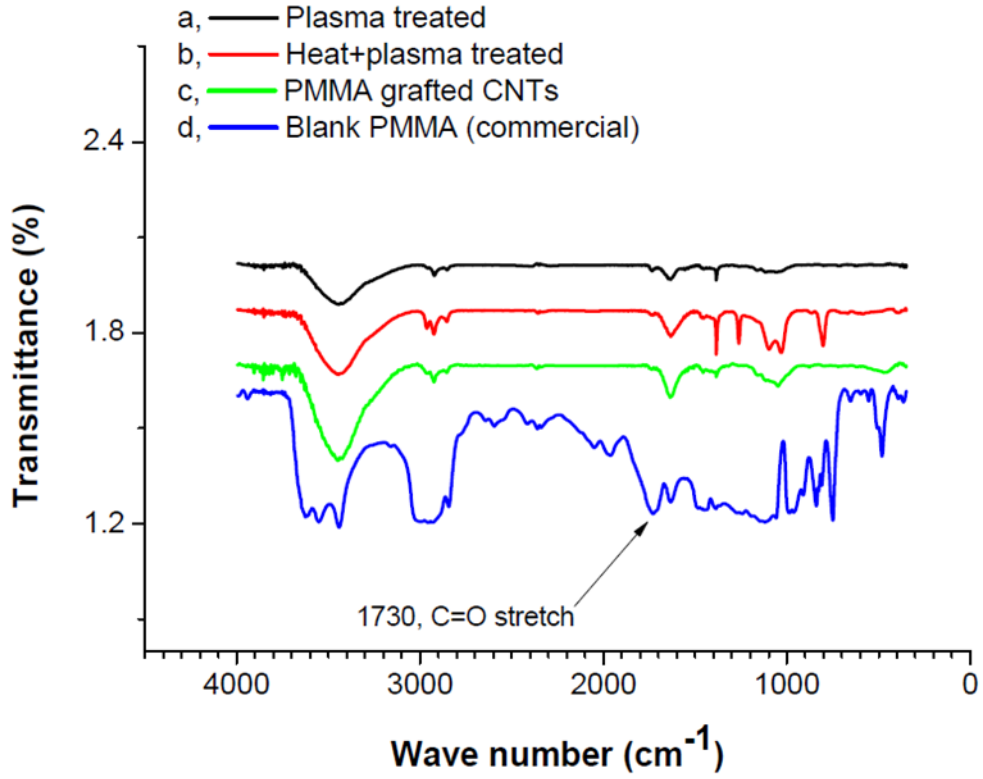

Figure 21: FTIR spectra of plasma treated VACNT (a), heat+plasma treated VACNT (b), PMMA grafted VACNT composite (c), and reference commercial PMMA (d) samples. Note: Although the FTIR spectrum of the blank PMMA prepared in our laboratory had shown more or less similar characteristic peaks as in the commercial PMMA, it is not presented here due to the presence of a significant amount of signal interference from water.

Comparatively, the reference PMMA and the VACNT/PMMA composite spectra contained more or less similar bands corresponding to the carbonyl, C=O stretch at 1730 cm^{-1}, C-O-C bending at 1189 cm^{-1}, methoxy, O-CH_3 stretch, and bending at 2992 cm^{-1} and 1450 cm^{-1}, Especially, since the methoxy signals are distinct to PMMA, the observed signals of the composite testified the presence of PMMA in the composite.

4.3.3. Proton nuclear magnetic resonance (^{1}H-NMR) analysis

The previous discussions based on the electron microscopy and FTIR analyses have revealed the presence of the polymer matrix (PMMA) surrounding the VACNTs. In addition, the FTIR study has also indicated the presence of carbonyl and methoxy groups due to carbonyl and methoxy stretching bands, respectively, which are characteristic bands of PMMA. To further confirm the presence of the grafted polymer chains in the composite, the VACNT/PMMA composite material was analyzed using ^{1}H-NMR and the results are shown in figure 22. The spectra are collected from the suspension of the samples prepared by sonication for 30 minutes in deuterated-chloroform.

Normally, the important signals for identifying PMMA are observed at chemical shift values 3.6, 1.5 and 1.2 ppm for methoxy hydrogen (-OCH_3), methylene hydrogen (-CH_2-) and hydrogens from methyl groups (-CH_3), respectively. Most often, the methoxy hydrogens (-OCH_3) are widely used for the identification of PMMA [101] and from the spectra in figure 22, the methoxy signals were observed around δ=3.6 for all samples. In addition to those peaks, some extra peaks associated with trace amount of methanol, ethanol and DMF, which are the solvents used during the preparation of the blank and VACNT/PMMA composite, are observed around 3.48, 3.72 & 1.24, and 2.9 ppm, respectively.

The ^{1}H-NMR signal of the methoxy group hydrogens observed for the composite prepared through GO-modified method is much weaker than the one prepared through CNF-modified method as well as the blank polymer. The weaker signal of the methoxy hydrogen for the composite prepared *via* GO-modified method might be associated with the effectiveness of the method in producing significantly detectable amount of grafted polymer matrix (PMMA) as already discussed in 4.3.1. On other hand, the composite prepared through the CNF-modified method showed comparatively more intense signals of the methoxy group hydrogens than the GO-method, as a result of more or longer polymer chains grafted on the nanotubes. This result is completely in agreement with the SEM images in Figure 19 (d).

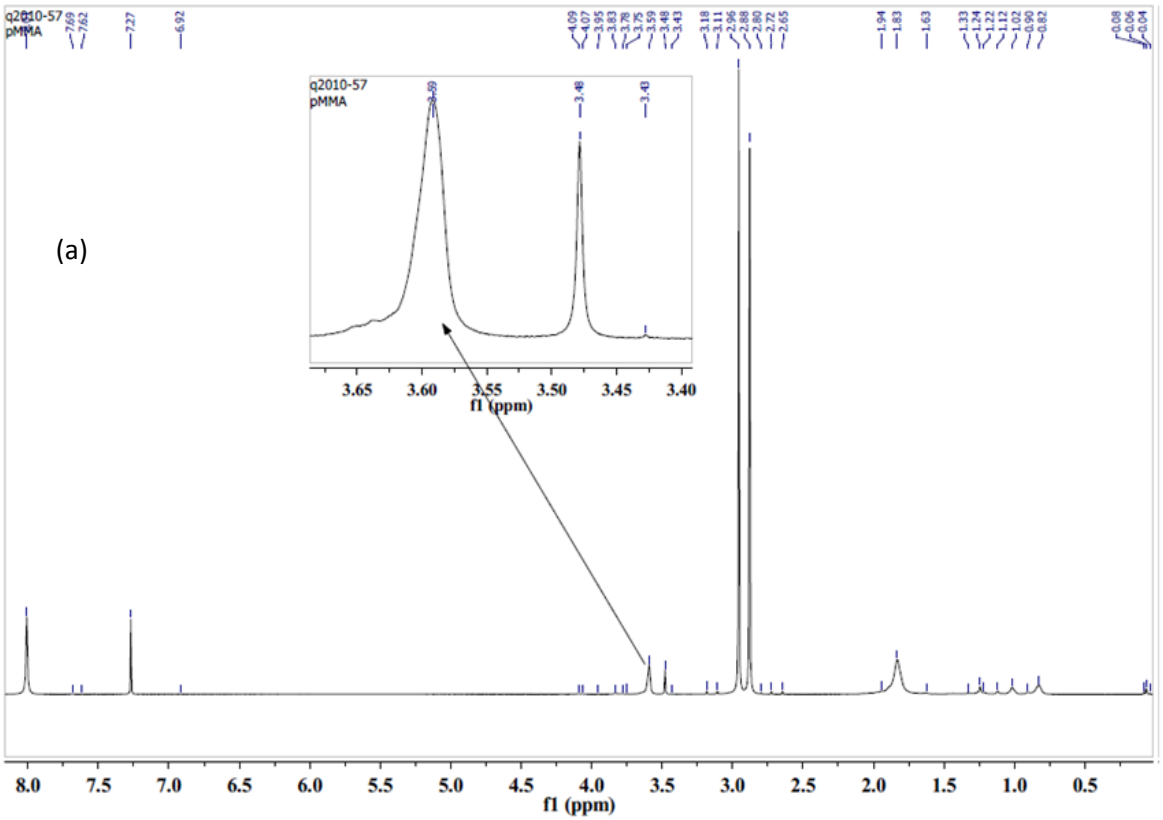
(a)
q2010-57
pMMA
f1 (ppm)

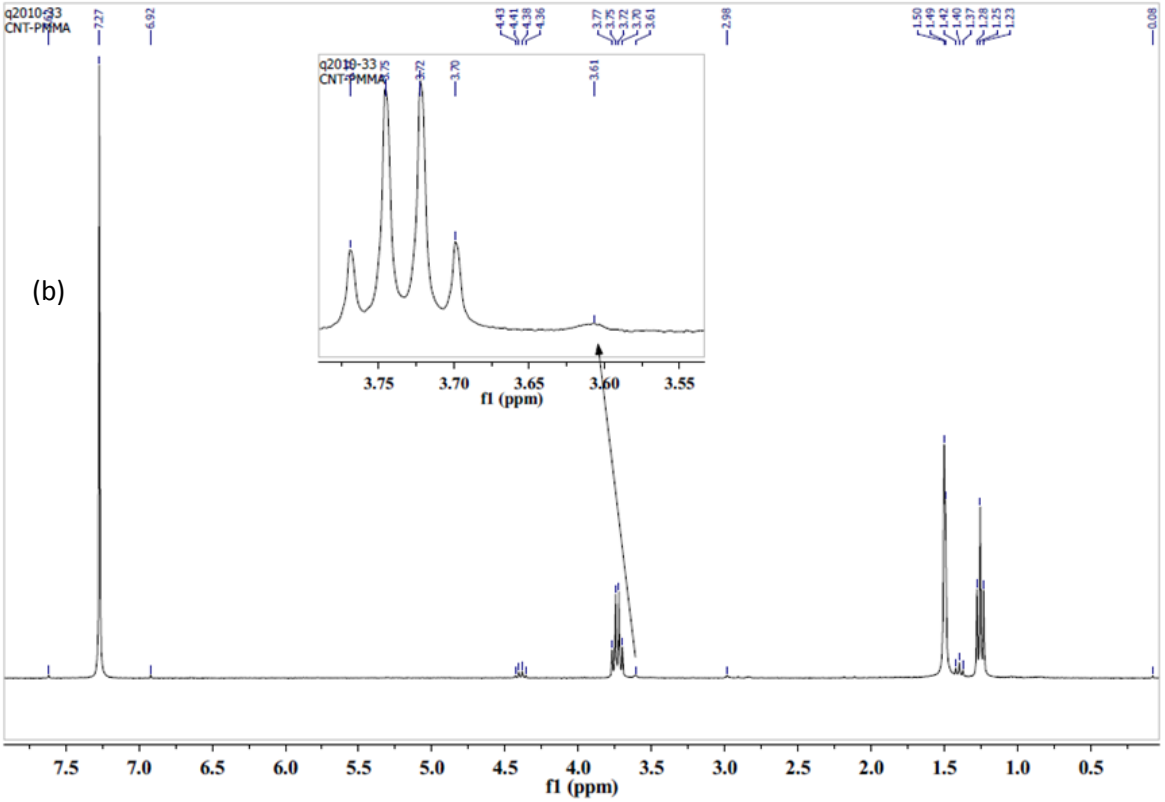
(b)
q2010-33
CNT-PMMA
f1 (ppm)

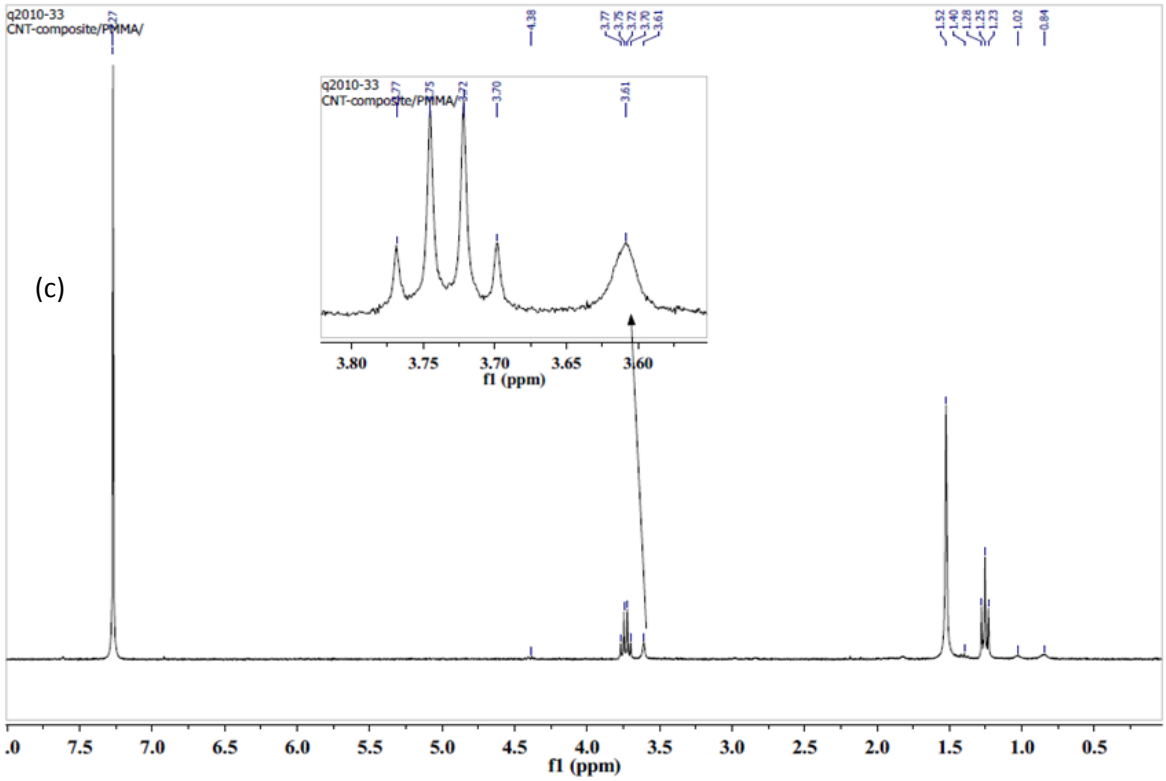

Figure 22: ^{1}H-NMR spectra of blank PMMA (a), which is plotted for comparison and that of VACNT/PMMA composites ^{1}H-NMR spectra prepared through GO-modified method (b) and CNF-modified method (c).

4.3.4. Miscellaneous comments on VACNT composites

In general, the SEM, FTIR and NMR studies have confirmed the presence of polymer matrix grafted on the VACNTs in the composite produced by ATRP using the CNF-modified route. Although the morphology of the composite *via* CNF-modified method caused more bundling and zippering of VACNTs to form a wedge-like morphology, it was found out to be the better ATRP polymerization method than the GO-modified route in modifying the surface of VACNTs with the polymer (PMMA). However, the GO-modified method despite preserving the VACNT morphology better than its counterpart, its composite was not rich in polymer. Perhaps this might be due to the shorter processing time spent in solution that helped in preserving its morphology whilst allowing the grafting of only limited amount of polymers. On the contrary, the composite prepared via the CNF-modified method was found to graft plenty of the PMMA polymers on the surface of the VACNTs. Unfortunately, the small amount of the composite samples produced in our work has hampered the determination of the molecular weight of the grafted PMMA chains

using gel permeation chromatography (GPC), which would provide us information regarding the chain length of the grafted polymers and also the determination of the amount of the polymers grafted using thermogravimetric analysis (TGA).

Figure 23: 5 mm×10 mm of the free standing VACNT/PMMA composite removed from the surface of the substrate prepared through CNF-modified method.

Eventually, the VACNT/PMMA composite material was further tested to check whether it could be lifted off from the surface of the substrate to get a free standing composite. Using a sharp blade it was shown that the composite material can be separated from its substrate to sustain itself independently as shown in figure 23.

Due to its porous nature and the ability to prepare free standing composite materials, as the one produced in our work, it could find an application as isoporous membrane for the filtering and purification of saline water, gases or selective separation of specific molecules [99]. VACNT membranes differ than other forms of filters such as activated carbon filters and zeolites in such a way that the internal hollow cavities of the CNTs are used as a channel for transporting the species to be separated [102]. The uniformity in the pore size and diameter control of the nanotubes have also allowed the passage of very small molecules without reducing the flow rate of the species passing through the cavities due to their frictionless, smooth structure and hydrophobic nature. Moreover, chemical modification of the nanotubes would allow selective gate-controlled separation of molecules [20]. Several papers have been published on this area of application and various

membrane preparation methods have been demonstrated [20, 102 and 103]. Usually, the following steps were followed to prepare the VACNT membrane filters.

- Grow vertically aligned CNTs on a substrate (silicon or quartz),
- Infiltrate the spaces between the CNTs with matrix materials such as polystyrene (PS) [20] and epoxy [103], and
- Remove the substrate and expose the nanotubes tips from the matrix through polishing, plasma or acid treatment [20, 104 and 105].

However, a different approach has also been followed by Yu et al for the preparation of such kind of membranes [102]. They have used solvent-induced collapse of VACNTs to prepare high density, vertically aligned CNTs with an average interstitial spacing of 3 nm as reported in Futaba et al. [46]. And, higher magnitude (~200 times) of gas permeation was reported than 10 nm PC membrane as a result of the additional interstitial pore permeation besides the permeation through the nanotubes.

In conclusion, a variety of other potential applications can be thought of for our VACNTs/PMMA hybrid material; however, further studies are still required regarding the control the amount of polymer grafted as well as the maintaining the integrity of the forests to yield a material with adequate mechanical properties.

4.4. Compression tests

Excellent mechanical properties (highest stiffness and modulus) of CNTs have already been established for CNTs by various authors [106, 107]. However, there is still an ongoing effort to understand the mechanical properties (compressive and tensile strength) of vertically aligned CNTs. Super compressible characteristic of ~1mm long VACNTs was reported by Cao et al via cyclic compression [108]. During the cyclic compression test wavelike folding of VACNT arrays has been observed due to multi-mode buckling. And the compressibility was reported to be as high as ~85 %. Additionally, the CNTs showed a linear elastic stage up to a critical strain (ε_c) of 53 % with a compressive Young´s modulus of 5.85 MPa. Beyond the critical strain the modulus increased exponentially due to the complete collapse of individual CNTs.

The mechanism for the compression test can be understood by considering the fundamental mode of buckling theory following the illustration in figure 24 [109]. Neglecting surface entanglement and interactions of CNTs with each other, each CNT can be modeled as an elastic column of length, L, with Young´modulus, E, and area moment of inertia, I. The VACNTs buckle during compression test if only a compressive force, F, applied exceeds the critical load, F_{cr}, given by:

$$F_{cr} = \alpha\, \pi^2\, EI/L^2 \tag{6}$$

Where, α is a non-dimensional factor that depends on boundary conditions. For a hollow cylinder the area moment of inertia, I, is given as:

$$I = \pi({R_o}^4 - {R_i}^4)/4 \tag{7}$$

Where R_o and R_i are the outer and inner radii of the column (CNTs). Equation 9 can be re-written by substituting I to equation 9 as:

$$F_{cr} = \alpha\, \pi^3\, E({R_o}^4 - {R_i}^4)/4L^2 \tag{8}$$

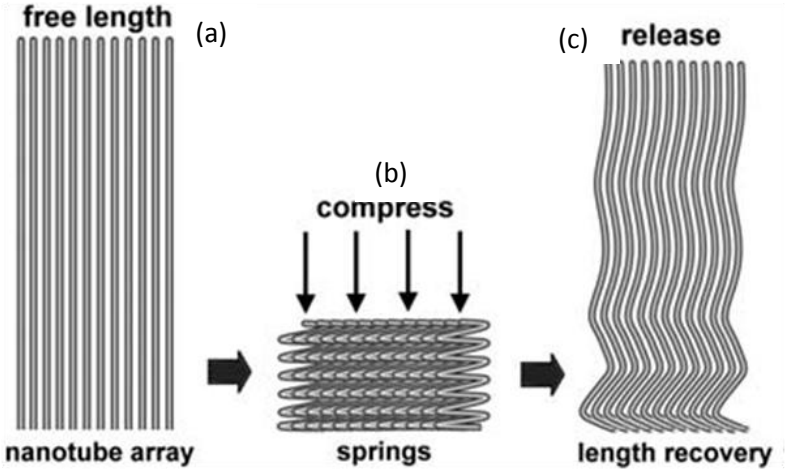

Figure 24: Schematic representation of compressive test for VACNT. (a) Free standing before compression, (b) buckled during compression and (c) springing back of VACNTs after compression [108].

Deck et al. [89] have investigated the mechanical properties of long mats of MWCNTs using Thermo-Mechanical Analyzer (TMA) and *in situ* testing in SEM. From both methods the compressive stiffness was reported to be ~820 MPa on average. The low stiffness was attributed to the buckling of the high aspect ratio CNTs. Furthermore, the

long MWCNTs mats produced through the CVD of benzene with constant addition of ferrocene were reported to give discontinuous CNTs. As a result the true individual lengths of the CNTs are much smaller than the total height of the mat. They have also related the low compressive stiffness of the VACNT mat to its structural make up.

On the other hand, compressive tests on vertically aligned MWCNTs array carried out by Tong et al [110] have shown only ~0.25 MPa compressive modulus for VACNTs of length 15, 40 and 500 μm. In addition they pointed out that the compressive modulus is independent of vertically aligned CNTs height up to 20 % of the strain recorded.

In relation to vertically grown CNTs, the composites of VACNTs find application in various areas such as aerospace and automotive industries, where high flexural rigidity and damping are critically important [111]. By introducing VACNTs into laminates, inter-laminar shear strength and fracture toughness of a laminate material could be enhanced.

Theoretically, composites would exhibit maximum damping when the reinforcing agents are oriented along the z-direction (through the thickness) of laminate composites. In the past, it has been extremely difficult to precisely control the alignment of the reinforcing agent in the z-direction. However, the possibility of growing vertically standing CNTs have created the opportunity to prove the theoretical claim regarding the achievement of maximum damping. On this regard, Zeng et al.[19] have prepared VACNT-based sandwich composite through vacuum assisted resin transfer mold (VARTM) and they reported high storage modulus of 19.8 GPa attributed to the alignment of CNTs. Furthermore, they have also reported a significant increase in the loss modulus as high as 0.5 GPa. Again they associated the high damping with the vertical alignment of CNTs in the composite.

In recent times, Ye at al. reported the grafting of PGMA from aligned MWCNTs using one-step initiated chemical vapor deposition (iCVD) [100]. In their work they transferred the modified aligned nanotubes by low temperature flip-over method to directly measure its mechanical properties using nanoindentation. They have reported a hardness of 0.49 GPa and an elastic modulus of 25.8 GPa for the modified VACNTs, while the pristine MWCNT was reported collapsed during the nanoindentation measurement. The PGMA coating was also reported to alleviate the collapse of the nanotubes by providing

mechanical support albeit the mechanical support was not strong enough to counterbalance the capillary force, which results in nanotube cluster. Yet, they have reported aligned structure, which was attributed to a synergistic effect created by the cross-linking of the grafted PGMA chains around the nanotubes and the formation of strong adhesion at the MWCNT/substrate interface.

Herein the VACNT/PMMA composite prepared via ATRP polymerization and pristine VACNTs were tested under static axial compression. Figure 25 depicts the compressive test result.

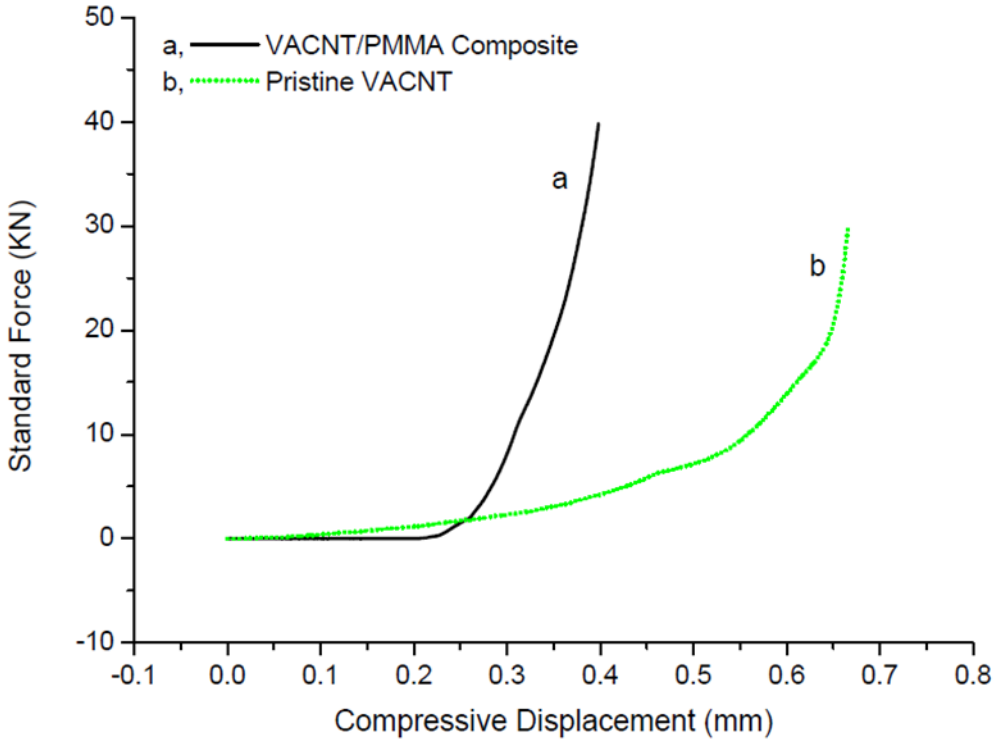

Figure 25: Compressive standard force vs compressive displacement of pristine VACNT/PMMA composite (a) and pristine VACNT (b).

The Compressive test on the pristine VACNT was carried out on ~1 mm long sample grown on a silicon substrate by CVD. For convenience the curve can be divided in three sections: from 0 to 0.47 mm, from 0.47 to 0.65 and from 0.65 to 0.66 mm. From 0 up to around 0.47 mm compressive displacement was caused by a standard force of roughly 7 KN. Standard forces of around 20 KN and 30 KN have compressive displacements of only 0.65 and 0.66 mm, respectively. In the first region, the VACNTs are compressed with ease causing the CNTs to buckle. Once the CNTs are buckled, a higher amount of standard

force is needed to deform the buckled carbon nanotubes together with the silicon substrate at which point a sharp rise in the standard force was observed.

On the other hand the PMMA modified VACNTs are shorter in length than the pristine VACNTs as a result of the zipping action caused by the solvents that forces the nanotubes to come close together. As a result, up to a compressive displacement of 0.21 mm the load was approaching the composite. It did not start pressing yet. It is only, after 0.21 mm onwards that the compressive force starts to act up on the sample. In fact, 0.21 mm can be regarded as the starting point and can be relabeled as zero compressive displacement. Here also the curve can be categorized into three regions: up to 0.21 mm, from 0.21 to 0.26 mm and from 0.26 to 0.4 mm. Up to 0.21 mm it is the pre-load stage. In the second region, roughly 0.05 mm displacement is caused by 2 KN of load on the composite. In the third region only 0.14 mm standard displacement is observed with a load of nearly 40 KN.

From the graph in figure 25, which shows the standard for as a function of displacement, it is obvious to understand that the pristine VACNTs are more compressive than the composite. This is expected because the modification of VACNTs with polymer has increased the density of the CNTs on the substrate through the "zipping effect" of the nanotubes. Moreover, the polymer matrix has also given an extra support to the VACNTs. This combination of VACNTs with polymer helps the CNTs to have a stable and rigid structural form supported by the polymer without losing their vertical alignment.

5. Conclusions and recommendations

Thermal CVD grown CNT forests have been successfully modified with PMMA *via* an *in situ* polymerization technique. To achieve this, an $Ar:O_2$ plasma was used to attach oxygen-containing functional groups on the surface of the VACNTs. From SEM studies and particularly from XPS, the presence of oxygen-containing functional groups (hydroxyl, carbonyl and carboxyl) has been confirmed. In addition, solubility tests have also showed that plasma treated and polymerized samples are dispersed better than the pristine VACNT in ethanol indicating the presence of polar functional groups attached. However, the percentage of oxygen in the nanotubes was low as indicated by the XPS analysis. The sample treated with both heat and plasma is found to have high purity as evidenced from the Raman study due to the removal of the amorphous carbon deposited on them. However, the heat treatment is found to oxidize the iron nanoparticles, which anchor the CNTs onto the substrate and the CNTs were easily eroded from the substrate in solution.

The hydroxyl groups produced from the plasma treatment were effectively modified with 2-bromo-2methylpropionylbromide (an ATRP initiator) for growing PMMA chains *via* ATRP from the surface of the VACNTs. Although parts of the CNT forests were found collapsed, a corrugated, wall like and denser composite structure has been produced as a result of solvent-induced zipping effect. The ATRP method has also been shown to be effectively used for grafting PMMA from the surface of the VACNTs as confirmed by STEM, FTIR and ^{1}H-NMR analysis. An improved compressive strength was also found for the VACNT/PMMA composite than the pristine VACNT as a result of the polymer matrix filling the spaces between the forests. The composite material produced was porous and it can be filled with other polymers or materials to produce a hybrid which contains aligned CNTs in it.

However, to maintain the structure of VACNTs it is advisable to avoid solvent system as much as possible. Therefore it is recommendable to use polymer infiltration technique to modify VACNTs with polymer directly. However, since infiltrations with polymer don´t create strong interfacial bonding as the covalent modification, the shear modulus might be compromised. Other modification methods, which involve less or no solvent such as

electrochemical modification and initiated chemical vapor deposition (iCVD) method seems to be promising and are recommendable.

In addition, the pre-heat treatment before the plasma modification was found to improve the quality of the VACNTs, by reducing the deposited amorphous carbon from their surface. It was also easier to scrap the VACNTs from the substrates due to the weakened connection from the oxidation of iron nano-particles that anchor the nanotubes on the substrate. Therefore, further studies can be made to prepare the composite of these continuous and substrate-free VACNTs using no or less solvent to reduce the damage of the vertically aligned CNTs as a result of processing in a solvent.

Moreover, the particle size of the iron catalysts used for growing the VACNTs might also have an influence in controlling the alignment of the nanotubes. Therefore, the influence of the catalyst particle size, which in turn controls the diameter of the nanotubes, towards maintaining the alignment of the nanotubes needs further investigation.

Despite the collapse of VACNTs inherent to the wet processing explored in this work, the honeycomb like structure VACNT/PMMA composite produced may find an interesting application as a membrane and damping agent in the areas of salt water desalination and, aircraft and automotive industries, respectively. The free standing frame work of the composite could also be infiltrated or filled by other materials including polymers to produce a hybrid containing aligned CNTs with an improved damping property.

6. References

1. Boehm, H. P.; "*The first observation of carbon nanotubes", Carbon*, **35** (4), (1997), 581.
2. Iijima, S.; "*Helical microtubules of graphitic carbon", Nature*, **354**, (1991) 56.
3. Iijima, S. and Ichihashi, T.; *"Single-shell carbon nanotubes of 1 nm diameter", Nature*, **363**, (1993), 603.
4. Bethune, D. S.; Klang, C. H.; de Vries, M. S.; Gorman, G.; Savoy, R.; Vazquez, J. and Beyers, R.; *"Cobalt-catalyzed growth of carbon nanotubes with single-atomic-layer walls", Nature*, **363**, (1993), 605.
5. Lu, J. P. and Han, J.; *"Carbon nanotubes and nanotube-based nano devices", Int. J. High Speed Elec. Sys*.; **9** (1998), 101
6. Baughman, R. H.; Zakhidov, A. A. and Zakhidov, W. A.; *"Carbon nanotubes-the route toward applications", Science*, **297**, (2002), 787.
7. Schnorr, J. M. and Swagger, T. M.; *"Emerging applications of CNTs", Chem. Mater.*, Article ASAP (2010). **DOI:** 10.1021/cm102406h
8. Dresselhaus, M. S.; Dresselhaus, G. and Eklund, P. C.; *Science of Fullerenes and Carbon Nanotubes*, Academic Press, San Diego, USA, (1995).
9. Smith, B. W. and Luzzi, D. E.; *Carbon Nanotubes; in Introduction to Nanoscale Science and Technology*, edited by Ventra, M. D., Evoy, S. and Helfin, (Jr.) J. R., Spring Science+Business Media, New York, USA, (2004), pp 137-182.
10. Meyyappan, M.; *"Carbon nanotubes: science and applications"*, CRC Press, Boca Raton, USA, 2005.
11. Han, J.; *Carbon Nanotubes: Science and Applications*, edited by Meyyappan M., CRC Press, Boca Raton, USA, (2005), pp2-21.
12. Harris, P. J. F.; *Carbon Nanotube Science: Synthesis, Properties and Application*, Cambridge University Press, New York, USA, (2009), p 52.
13. Serp, P., and Figueredo, J. L.; *Carbon materials for catalysis*, John Wiley and Sons Inc., New Jersey, 2009.
14. White, C. J. and Todorov, T. N.; "*Carbon nanotubes as long ballistic conductors", Nature*, **393**, (1998), 240.

15. Berber, S.; Kwon, Y. -K. and Tománek, D.; *"Unusually high thermal conductivity of carbon nanotubes"*, *Phys. Rev. Let.*, **84** (20), (2000), 4613.
16. Saito, R.; Dresselhaus, G. and Dresselhaus, M. S.; *Physical Properties of Carbon*, Imperial College Press, London, 1998.
17. Frackowiak, E.; Jurewicz, K., Delpeux, L. and Béguin, F.; *"Nanotubular materials for supercapacitors"*, *J. Power Sour.*, **97-98**, (2001), 822.
18. Saito, Y. and Uemura, S.; *"Field emission from carbon nanotubes and its applications to electron sources"*, *Carbon*, **38**, (2000), 169.
19. Zeng, Y.; Ci, L.; Carey, B. J.; Vajtai, R. and Ajayan, P. M.; *"Design and reinforcement: vertically aligned carbon nanotube based sandwich composites"*, *ACS Nano*, article ASAP (2010). **DOI:** 10.1021/nn101650p.
20. Hinds, B. J.; Chopra, N.; Andrews, R..; Gavalas, V. and Bachas L. G.; *"Aligned multiwalled carbon nanotube membranes"*, *Science*, **303**, (2004), 62.
21. Yurdumakan, B.; Raravikar, N. R.; Ajayan, P. M. and Dhinojwala, A.; *"Synthetic gecko foot-hairs from multiwalled carbon nanotubes"*, *Chem. Commun.*, **30**, (2005), 3799.
22. Dai, H.; *"Carbon nanotubes: Synthesis, integration and properties"*, *Acc. Chem. Res.*, **35** (2002), 1035.
23. Rusling, J. F.; Yu, X.; Munge, B. S.; Kim, S. N. and Papadimitrakopoulos, F.; *Single-wall Carbon Nanotube Forests in Biosensors; In Engineering the Bioelectronic Interface: Applications to Analyte Biosensing and Protein Detection*, edited by Davis, J., The Royal Society of Chemistry, Science Park, UK, (2009), pp 94-118.
24. Chakrabarti, S.; Kume, H.; Pan, L. J.; Nagasaka, T. and Nakayama, Y.; *"Number of walls controlled synthesis of milimetr-long vertically aligned brushlike carbon nanotubes"*, *J. Phys. Chem. C*, **111**, (2007), 1929.
25. Hahm, M. G.; Kwon, Y-. K.; Lee, E.; Ahn, C. W. and Jung, Y. J.; *"Diameter selective growth of vertically aligned growth of single walled carbon nanotubes and study on their growth mechanism"*, *J. Phys. Chem. C*, **112**, (2008), 17143.
26. Hong, S. and Myung, S.; *"Nanotube electronics: A flexible approach to mobility"*, *Nature Nanotechnology*, **2** (4), (2007), 207.

27. Takesue, I.; Haruyama, J.; Kobayashi, N.; Chiashi, S.; Maruyama, S.; Sugai, T. and Shinohara, H.; *"Superconductivity in entirely end-bonded MWNTs"*, *Phys. Rev. Lett.*, **96** (5), (2006), 57001.
28. Barone, P. W.; Baik, S.; Heller, D. A. and Strano, M. S.; *"Near-infrared optical sensors based on single-walled carbon nanotubes"*, *Nature Mater.*, **4** (2005), 86.
29. Garg, A.; Han, J. and Sinnot, S. B.; *"Interactions of carbon-nanotubule proximal probe tips with diamond and graphene"*, *Phys. Rev, Lett.*, **81** (1998), 2260.
30. Qi, H. J.; Teo, K. B. K.; Lau, K. K. S.; Boyce, M. C.; Milne, W. I.; Robertson, J. and Gleason, K. K.; *"Determination of mechanical properties of carbon nanotubes and vertically aligned carbon nanotube forest using nanoindentation"*, *J. Mech. Phys. Solids*, **51**, (2003), 2213
31. Yi, W.; Lu, L.; Dian-lin, Z.; Pan, Z. W. and Xie, S. S.; *"Linear specific heat of carbon nanotubes"*, *Phys. Rev. B*, ***59*** (1999), R9015.
32. Hone, J.; Whitney, M.; Piskoti, C. and Zettl, A.; *"Thermal conductivity of single-walled carbon nanotubes"*, *Phys. Rev. B*, **59**, (1999), R2514.
33. Kim, P.; Shi, L.; Majumdar, A. and McEuen, P. L.; *"Thermal transport measurements of individual multiwalled nanotubes"*, *Phys. Rev. Lett.*, **87** (2001), 215502.
34. Yang, D. J.; Zhang, Q.; Chen, G.; Yoon, S. F.; Ahn, J.; Wang, S. G.; Zhou, Q.; Wang, Q. and Li, Q.; *"Thermal conductivity of multiwalled carbon nanotubes"*, *Physical Review B*, **66**, (2002), 165440.
35. Ebbesen, T. W.; In *Carbon Nanotubes: Preparation and Properties*, edited by Ebbesen, T. W., CRC Press, Boca Raton, USA, (1997), pp136-162.
36. Andrews, R.; Jacques, D.; Qian, D. and Dickey, E. C.; *"Purification and structural annealing of multiwalled carbon nanotubes at graphitization temperatures"*, *Carbon*, **39** (2001), 1681.
37. Kong, J.; Soh, H.; Cassell, A.; Quate, C. F. and Dai, H.; *"Synthesis of individual single-walled carbon nanotubes on patterned silicon wafers"*, *Nature*, **395** (1998), 878.
38. Su, M.; Zheng, B. and Liu, J.; *"A scalable CVD method for the synthesis of single-walled carbon nanotubes with high catalyst productivity"*, *Chem. Phys. Lett.*, **322** (2000), 321.

39. Maruyama, S.; Kojima, R.; Miyauchi, Y.; Chiashi, S. and Kohno M.; *"Low-temperature synthesis of high-purity single-walled carbon nanotubes from alcohol", Chem. Phys. Lett.*, **360** (2002), 229.
40. Nikolaev, P.; Bronikowski, M. J.; Bradley, R. K.; Rohmund, F.; Colbert, D. T.; Smith, K. A. and Smalley R. E.; *"Gas-phase catalytic growth of single-walled carbon nanotubes from carbon monoxide", Chem. Phys. Lett.*, **313** (1999), 91.
41. Joselevich, E.; Dai, H.; Liu, J.; Hata, K. and Windle, A. H.; *Carbon Nanotube Synthesis and Organization; In Carbon Nanotubes: Topics Appl. Physics*, edited by Jorio, A.; Dresselhaus, G. and Dresselhaus, M. S., **111** (2008), pp 101-164.
42. Li, J.; Papadopoulos, C.; Xu, J. M. and Moskovit M.; *"Highly-ordered carbon nanotube arrays for electronics applications", Appl. Phys. Lett.*, **75** (1999), 367.
43. Hata, K.; Futaba, D. N.; Mizuno, K.; Namai, T.; Yumura, M. and Iijima, S.; *"Water-assisted highly efficient synthesis of impurity-free single-walled carbon nanotubes", Science*, **306**, (2004), 1362.
44. Chandrashekar, A.; Ramachandran, S.; Pollack, G. P.; Lee, J. S.; Lee, G. S. and Overzet, L. J.; *"Forming carbon nanotube composites by directly coating forests with inorganic materials using low pressure chemical vapor deposition", Thin solid films*, **517** (2008), 525.
45. Ren, Z. F.; Huang, Z. P.; Xu, J. W.; Wang, J. H.; Bush, P.; Siegel, M. P. and Provencio, P. N.; *"Synthesis of large arrays of well-aligned carbon nanotubes on glass", Science*, **282** (1998), 1105
46. Futaba, D. N.; Hata, K.; Namai, T.; Yamada, T.; Mizuno, K.; Hayamizu, Y.; Yumura, M. and Iijima, S.; *"84% catalyst activity of water-assisted growth of single waledl carbon nanotube forest characterization by a statistical and macroscopic approach", J. Phys. Chem. B*, **110**, (2006), 8035.
47. Banerjee, S.; Hemraj-Benny, T. and Wong, S. S.; *"Covalent surface chemistry of single-walled carbon nanotubes", Adv. Mater.*, **17** (2005) 17.
48. Karousis, N. and Tagmatarchis, N.; *"Current progress on the chemical modification of carbon nanotubes", Chem. Rev.*, **110**, (2010), 5366.
49. Mickelson, E. T.; Huffman, C. B.; Rinzler, A. G.; Smalley, R. E.; Hauge, R. H. and Margarave, J. L.; *"Fluorination of single-wall carbon nanotubes", Chem. Phys. Lett.*, **296**, (1998), 188.

50. Chen, Y.; Haddon, R. C.; Fang, S.; Rao, A. M.; Eklund, P. C.; Lee, W. H.; Dickey, E. C.; Grulke, E. A.; Pendergrass, J. C.; Chavan, A.; Haley, B. E. and Smalley, R. E.; *"Chemical attachment of organic functional groups to single-walled carbon nanotube material", J. Mater. Res.*, **13**, (1998), 2423.
51. Holzinger, M.; Vostrowsky, O.; Hirsch, A.; Hennrich, F.; Kappes, M.; Weiss, R. and Jellen, F.; *"Sidewall functionalization of carbon nanotubes", Angew. Chem. Int. Ed*., **40**, (2001), 4002.
52. Holzinger, M.; Abraham, J.; Whelan, P.; Graupner, R.; Ley, L.; Hennrich, F.; Kappes, M. and Hirsch, A.; *"Functionalization of single-walled carbon nanotubes with (R-)oxycarbonyl nitrenes", J. Am. Chem. Soc.*, **125**, (2003), 8566.
53. Georgakilas, V.; Kordatos, K.; Prato, M.; Guldi, D. M.; Holzinger, M. and Hirsch, A.; *"Organic functionalization of carbon nanotubes", J. Am. Chem. Soc.*, **124**, (2002), 760.
54. Maggini, M.; Scorrano, G. and Prato, M.; *"Addition of azomethine ylides to C60: synthesis, characterization, and functionalization of fullerene pyrrolidines", J. Am. Chem. Soc.*, **115**, (1993), 9798.
55. Viswanathan, G.; Chakrapani, N.; Yang, H.; Wei, B.; Chung, H.; Cho, K.; Ryu, C.and Ajayan, P.; *"Single-step in situ synthesis of polymer-grafted single-wall nanotube composites", J. Am. Chem. Soc.*, **125**, (2003), 9258.
56. Liang, F.; Sadana, A. K.; Peera, A.; Chattopadhyay, J.; Gu, Z.; Hauge, R. H. and Billups, W. E.; *"A convenient route to functionalized carbon nanotubes", Nano Letters*, **4**, (2004), 1257.
57. Pastine, S. J.; Okawa, D.; Kessler, B.; Rolandi, M.; Llorente, M.; Zettl, A. and Frechet, J. M. J.; *"A facile and patternable method for the surface modification of carbon nanotube forests using perfluoroarylazides", J. Am. Chem. Soc.,* **130**, (2008), 4238.
58. Yang, W. R.; Thordarson, P.; Gooding, J. J.; Ringer, S. P. and Braet, F.; *"Carbon nanotubes for biological and biomedical applications", Nanotechnology*, **18**, (2007), 412001.
59. Liu, J. Q.; Chou, A.; Rahmat, W.; Paddon-Row, M. N. and Gooding, J. J; *"Achieving direct connection to glucose oxidase using aligned single walled carbon nanotube arrays", Electroanalysis*, **17**, (2005), 38.

60. Liu, J.; Rinzler, A. G.; Dai, H.; Hafner, J. H.; Bradley, R. K.; Boul, P. J.; Lu, A.; Iverson, T.; Shelimov, K.; Huffman, C. B.; Rodriguez-Macias, F.; Shon, Y. S.; Lee, T. R.; Colbert, D. T. and Smalley, R. E.; *"Fullerene pipes", Science*, **280**, (1998), 1253.
61. Mawhinney, D. B.; Naumenko, V.; Kuznetsova, A.; Yates, J. T.; Liu, J. and Smalley, R. E.; *"Infrared spectral evidence for the etching of carbon nanotubes: Ozone oxidation at 298 K", J. Am. Chem. Soc.*, **122**, (2000), 2383.
62. Chen, J.; Hamon, M. A.; Hu, H.; Chen, Y.; Rao, A. M.; Eklund, P. C. and Haddon, R. C.; *"Solution properties of single-walled carbon nanotubes", Science*, **282**, (1998), 95.
63. Hamon, M. A.; Hui, H.; Bhowmik, P.; Itkis, H. M. E. and Haddon, R. C.; *"Ester-functionalized soluble single-walled carbon nanotubes", Appl. Phys. A*, **74**, (2002), 333.
64. Lim, J. K.; Yun, W. S.; Yoon, M.; Lee, S. K.; Kim, C. H.; Kim, K. and Kim, S. K.; *"Selective thiolation of single-walled carbon nanotubes", Synth. Met.*, **139**, (2003), 521.
65. Bahr, J. L.; Yang, J.; Kosynkin, D. V.; Bronikowski, M. J.; Smalley, R. E. and Tour, J. M.; *"Functionalization of carbon nanotubes by electrochemical reduction of aryl diazonium salts: A bucky paper electrode", J. Am. Chem. Soc.*, **123**, (2001), 6536.
66. Ye, J-. S.; Wen, Y.; Zhang, W-. D.; Cui, H. F.; Xu, G. Q. and Sheu, E-. S.; *"Electrochemical functionalization of vertically aligned carbon nanotube arrays with molybdenum oxides for the development of a surface-charge-controlled sensor", Nanotechnology*, **17**, (2006), 3994
67. Ye, X. R.; Chen, L. H.; Wang, C.; Aubuchon, J. F.; Chen, I. C.; Gapin, A. I.; Talbot, J. B. and Jin, S.; *"Electrochemical modification of vertically aligned carbon nanotube arrays", J. Phys. Chem. B*, **110**, (2006), 12938.
68. Huang, S. and Dai, L.; *"Plasma etching for purification and controlled opening of aligned carbon nanotubes", J. Phys. Chem. B*, **106**, (2002), 3543.
69. Xu, T.; Yang, J.; Liu, J. and Fu, Q.; *"Surface modification of multi-walled carbon nanotubes by O2 plasma", Appl. Surface Sci.*, **253**, (2007), 8945.

70. Chen, Q.; Dai, L.; Gao, M.; Huang, S. and Mau, A.; *"Plasma activation of carbon nanotubes for chemical modification", J. Phys. Chem.*, **105**, (2001), 618.
71. Khare, B. N.; Wilhite, P.; Quinn, R. C., Chen, B.; Schingler, R. H.; Tran, B.; Imanaka, H.; So, C. R.; Bauschlicher, C. W. and Meyyappan, M.; *"Functionalization of carbon nanotubes by ammonia glow-discharge: Experiments and modeling", J. Phys. Chem. B*, **108**, (2004), 8166.
72. Vohrer, U.; Zschoerper, N. P.; Koehne, Y.; Langowski, S. and Oehr, C.; *"Plasma modification of CNT and bucky paper", Plasma Process Polym.*, **4**, (2007), S871.
73. Zschoerper, N. P.; Katzenmaier, V.; Vohrer, U.; Haupt, M.; Oehr, C. and Hirth, T.; *"Analytical investigation of the composition of plasma-induced functional groups on carbon nanotube sheets", Carbon,* **47** (2009) 2174.
74. Kristic, V.; Duesberg, G. S.; Muster, J.; Burghard, M. and Roth, S.; *"Langmuir-Blodgett films of matrix-diluted single-walled carbon nanotubes", Chem. Mater.*, **10** (1998), 2338.
75. Islam, M. F.; Rojas, E.; Bergey, D. M.; Johnson, A. T. and Yodh, A. G.; *"High weight fraction surfactant solubilization of single-wall nanotubes in water", Nano Lett.*, **3** (2003) 269.
76. In het Panhuis, M.; Salvador-Morales, C.; Franklin, E.; Chambers, G.; Fonseca, A.; Nagy, J. B.; Blau, W. J. and Minett, A. I.; *"Characterization of an interaction between functionalized carbon nanotubes and an enzyme", J. Nanosci. Nanotechnol.*, **3** (2003) 209.
77. Zhao, J.; Lu, J. P.; Han, J. and Yang, C. K.; *"Non-covalent functionalization of carbon nanotubes by aromatic organic molecules", Appl. Phys. Lett.*, **82** (2003) 3746.
78. O´Connell, M. J.; Boul, P.; Ericson, L. M.; Huffman, C.; Wang, Y.; Haroz. E.; Kuper, C. and Smalley, R. E.; *"Reversible water-solubilization of single-walled carbon nanotubes by polymer wrapping", Chem. Phys. Lett.*, **342** (2001) 265.
79. Ajayan, P. M.; Stephan, O.; Colliex, C. and Trauth, D.; *"Aligned carbon nanotube arrays formed by cutting a polymer-resin nanotube composite", Science*, **265** (1994) 1212.

80. Spitalsky, Z.; Tasis, D.; Papagelis, K. and Galiotis, C.; *"Carbon nanotube polymer composites: Chemistry, processing, mechanical and electrical properties", Prog. Polym. Sci.*, **35** (2010) 357.
81. Braunecker, W. A. and Matyjaszewski, K.; *"Controlled/living radical polymerization: Features, developments and perspectives", Prog. Polym. Sci*., **32** (2007) 93.
82. Yao, Z.; Braidy, N.; Botton, G. A. and Adronov, A.; *"Polymerization from the surface of single-walled carbon nanotubes-preparation and characterization of nanocomposites", J. Am. Chem. Soc.*, **125,** (2003) 16015.
83. Baskaran, D.; Mays, J. W. and Bratcher, M. S.; *"Polymer-grafted multiwalled carbon nanotubes through surface-initiated polymerization", Angew. Chem. Int. Ed.*, **43,** (2004) 2138.
84. Sun, T.; Liu, H.; Song, W.; Wang, X.; Jiang, L.; Li, L. and Zhu, D.; *"Responsive aligned carbon nanotubes", Angew. Chem. Int. Ed*., **43,** (2004) 4663.
85. Matrab, T.; Chancolon, J.; L'hermite, M. M.; Rouzaud, J. N.; Deniau, G.; Boudou, J. P.; Chehimi, M. M. and Delamar, M.; *"Atom transfer radical polymerization (ATRP) initiated by aryl diazonium salts: A new route for surface modification of multiwalled carbon nanotubes by tethered polymer chains", Colloids Surf. Physicochem. Eng. Asp.*, **287,** (2006) 217.
86. Lee, S. H.; Dreyer, D. R.; An, J.; Velamakanni, A.; Piner, R. D.; Park, S.; Zhu, Y.; Kim, S. O.; Bielawski, C. W. and Ruoff, R. S.; *"Polymer brushes via controlled, surface-initiatedatom transfer radical polymerization (ATRP) from graphene oxide", Macromol Rapid Commun.*, **30** (2009). DOI: 10.1002/marc.200900641.
87. Ghislandi, M.; de A.Prado, L. A. S.; de la Vega Oyerviedes, A.; Wittich, H.; Schulte, K. and Barros-Timmons, A.; *"Functionalization of carbon nanofibers (CNFs) through atom transfer radical polymerization for the preparation of poly(tert-butyl acrylate)/CNF materials: Spectroscopic, thermal, morphological and physical characterizations", J. Polym. Sci., Part A: Polym. Chem.*, **46** (2008) 3326.
88. Nessim, G. D.; Hart, A. J.; Kim, J. S.; Acquaviva, D.; Oh, J.; Morgan, C. D.; Seita, M.; Leib, J. S. and Thompson, C. V.; *"Tuning of vertically-aligned carbon*

nanotube diameter and areal density through catalyst pre-treatment", Nano Lett., **8**, (2008), 3587

89. Deck, C. P.; Flowers, J.; Mckee, G. S. B. and Vecchio K.; *"Mechanical behavior of ultra-long multiwalled carbon nanotube mats", J. Appl. Phys.*, **101** (2007), 023512.
90. Xu, L.; Fang, Z.; Song, P. and Peng, M.; *"Surface-initiated graft polymerization on multiwalled carbon nanotubes pretreated by corona discharge at atmospheric pressure", Nanoscale*, **2,** (2010), 389.
91. Chattopadhyay, J.; Cortez, F. de J.; Chakraborty, S.; Slater, N. K. H. and Billup, W. E.; *"Synthesis of water solublePEGylatedsingle-walled carbon nanotubes", Chem. Mater.*, 18, (2006), 5864.
92. Costa, S.; Borowiak-Palen, E.; Kruszyñska, M.; Bachmatiuk, A. and Kaleńczuk, R. J.; *"Characterization of carbon nanotubes by Raman spectroscopy", Material Science of Poland*, **26** (2008), 433.
93. Antones, E. F.; Almeida, E.C.; Rosa, C. B.; de Medeiros, L. I.; Pardini, L. C.; Massi, M. and Corat, E. J.; *"Thermal annealing and electrochemical purification of multi-walled carbon nanotubes produced by camphor/ferrocene mixtures", J. Nanosci. Nanotechnol.*, **10** (2010) 1296.
94. Souza, M.; Jorio, A.; Fantini, C.; Neves, B. R. A.; Pimenta, M. A.; Saito, R.; Ismach, A.; Joselevich, E.; Brar, V. W.; Samsonidze, Ge. G.; Dresselhaus, G. and Dresselhaus, M. S.; *"Single- and double-resonancce Raman G-band processes in carbon nanotubes", Phys. Rev. B*, **69** (2004) 241403(R).
95. Nan, X.; Gu, Z. and Liu, Z.; *"Immobilizing shortened single-walled carbon nanotubes (SWNTs) on gold using a surface condensation technique", J. Colloid Interface Sci.*, 245, (2002), 311.
96. Chatopadhyay, D.; Galeska, I. and Papadimitrakopoulos, F.; *"Metal-assisted organization of shortened carbon nanotubes in monolayer and multilayer forest assemblies", J. Am. Chem. Soc.,* 123, (2001), 9451.
97. Dillon, A. C.; Yudasaka, M. and Dresselhaus, M. S.; *"Employing Raman spectroscopy to qualitatively evaluate carbon single-wall nanotube materials" J. Nanosci. Nanotechnol.*, **4,** (2004) 691.

98. http://www.cmu.edu/maty/chem/fundamentals-atrp/index.html, accessed at 17:30, on the 3rd of December, 2010.
99. Gross, S.; Camozzo, D.; Di Noto, V.; Armelao, L. and Tondello, E.; *"PMMA: A key macromolecular component for dielectric low-κ hybrid inorganic-organic polymer films", Eur. Polym. J.*, **43,** (2007) 673.
100. Ye, Y.; Mao, Y.; Wang, F.; Lu, H.; Qu, L. and Dai, L.; *"Solvent-free functionalization and transfer of aligned carbon nanotubes with vapor-deposited polymer nanocoatings", J. Mater. Chem.,* (2010). **DOI**: 10.1039/c0jm02506b.
101. Mirau, P. A.; *NMR Characterization of Polymers; in Polymer Characterization*, edited by Hunt, B. J. and James, M. I., Blackie Academic and Professional, Glasgow, UK, (1993), PP 37-68.
102. Yu, M.; Funke, H. H.; Falconer, J. H. and Noble, R. D.; *"High density, vertically-aligned carbon nanotube membranes", Nanolett.,* **9**, (2009), 225.
103. Sears, K.; Dumée, L.; Scutz, J.; She, M.; Huynh, C.; Hawkins, S.; Duke, M. and Gray, S.; *"Recent developments in carbon nanotube membranes for water purification and gas separation", Materials,* **3**, (2010), 127.
104. Holt, J. K.; Park, H. G.; Wang, Y.; Staderman, M.; Artyukhin, A. B.; Grigoropoulos, C. P.; Noy, A. and Bakajin, O.; *"Fast Mass Transport Through Sub-2-Nanometer Carbon Nanotubes". Science*, **312**, (2006), 1034.
105. Mi, W.; Lin, Y. S. and Li, Y.; *"Vertically Aligned Carbon Nanotube Membranes on Macroporous Alumina Supports", J. Membr. Sci.*, **304**, (2007), 1.
106. Yu, M. F.; Lourie, O.; Dyer, M. J.; Moloni, K.; Kelly, T. F. and Ruoff, R. S.; *"Strength and breaking mechanism of multiwalled carbon nanotubes under tensile load", Science,* **287,** (2000) 637.
107. Zhang, Y. Q.; Liu, G. R. and Wang, J. S.; *"Small-scale effects on buckling of multiwalled carbon nanotubes under axial compression", Phys. Re*V. *B*, **70**, (2004) 205430.
108. Cao, A.; Dickrell, P. L.; Sawyer, W. G.; Ghasemi-Nejhad, M. N. and Ajayan, P. M.; "*Super-compressible foam-like films of carbon nanotubes", Science*, **310** (2005), 1307.
109. Timoshenko, S. P.; *Theory of elastic stability*, McGraw Hill Book Co., New York, (1961).

110. Tong, T.; Zhao, Y.; Delzeit, L.; Kashani, A.; Meyyappan, M and Majumdar A.; *"Height independent compressive modulus of vertically aligned carbon nanotube arrays", Nanolett.*, **8**, (2008), 511.
111. Finegan, I. C. and Gibson, R. F.; *"Recent research on enhancement of damping in polymer composites", Compos. Struct.*, **44,** (1999), 89.